UNIVERSITY OF CALIFORNIA SAN DIEGO

Directed Conversion of Human Retinal Ganglion Cells by Overexpression of Transcription Factors

A thesis submitted in partial satisfaction of the requirements
for the degree of Master of Science

in

Biology

by

Ryan Mitchel Wong

Committee in charge:

Professor Karl Wahlin, Chair
Professor Michael Perry, Co-Chair
Professor David Traver
Professor Karl Willert

2020

The Thesis of Ryan Mitchel Wong is approved, and it is acceptable in quality and form for publication on microfilm and electronically:

_____

_____

_____

_____

Chair

University of California San Diego

2020

DEDICATIONS

Dedicated to my parents for supporting my education and instilling an early interest in ophthalmology.

TABLE OF CONTENTS

LIST OF FIGURES

LIST OF TABLES

3G-TRE	TET response element
APC	Adenomatosis polyposis coli
ATOH7	Atonal 7
Ascl1	Achaete-scute homolog 1
Ascl1a	Achaete-scute homolog 1a
BDNF	Brain-derived Neurotrophic Factor
BMP	Bone Morphogenic Protein
BMP7	Bone Morphogenic Protein 7
BRN3B / POU4F2	Brain-3B
CK1α	Casein kinase 1α
CNTF	Ciliary Neurotrophic Factor
Cbh	Chicken beta-actin hybrid
DMSO	Dimethyl sulfoxide
Dox/Doxy	Doxycycline
DM	Differentiation Medium
ECM	Extracellular matrix
FGF	Fibroblast Growth Factors
FZD	Frizzled receptor
GSK3	Glycogen synthase kinase 3
Gli	Glioma-associated oncogene homolog
HDR	Homology directed repair
IGF	Insulin-like Growth factors
INL	Inner nuclear layer
IPL	Inner plexiform layer
ISL1	Islet-1
LATS1/2	Large Tumor Suppressor Kinase 1/2
LB	Lysogeny broth
LRP5/6	Low-density lipoprotein receptor-related protein 5/6
MAP4K	Mitogen-Activated Protein Kinase Kinase Kinase Kinase
MG	Müller glia
MST1/2	Mammalian STE20-Like Protein Kinase 1/2
NAIB	NGN2, ATOH7, ISL1, and BRN3B
NEB	New England Biolabs
NGN2 / NEUROG2	Neurogenin-2
NIM	Neural Induction Medium
ONL	Outer nuclear layer
OPL	Outer plexiform layer
PAM	Protospacer adjacent motif
PCR	Polymerase chain reaction
PP2A	Protein phosphatase 2A
PSC	Pluripotent stem cell

Ptch1	Patched
R-Smads	Receptor-regulated Smads
RGC	Retinal ganglion cell
RPE	Retinal pigment epithelium
Shh	Sonic hedgehog
Smo	Smoothened
Sox	Sry-related high mobility box
SOX2	Sex determining region Y-box 2
TAZ	Transcriptional Co-Activator with PDZ-Binding Motif
TEAD 1-4	TEA Domain transcription factors
TET	Tetracycline
TGF- β	Transforming Growth Factor β
Tm	primer melting temperature
YAP	Yes Associated Protein
cDNA	Complementary DNA
gDNA	Genomic DNA
gRNA	Guide RNA
iPSC	Induced pluripotent stem cell
rtTA	Reverse tetracycline trans-activating sequence

ACKNOWLEDGMENTS

I would like to acknowledge Professor Karl Wahlin for both his mentorship as my principal investigator, and his support as the chair of my committee. His overwhelming patience and guidance made me a better scientist. He pushed me to work harder, think critically, and challenge my limits.

I would also like to acknowledge the members of the Wahlin Lab, past and present. I really appreciate their support and assistance throughout my time working in this lab.

ABSTRACT OF THE THESIS

Directed Conversion of Human Retinal Ganglion Cells by Overexpression of Transcription Factors

by

Ryan Mitchel Wong

Master of Science in Biology

University of California San Diego, 2020

Professor Karl Wahlin, Chair

Professor Michael Perry, Co-Chair

While some vertebrate species such as zebrafish have demonstrated a robust repair and regeneration ability, the extent of this regenerative capacity in mammals is limited. In humans, it is unknown whether this process even occurs. Vision loss resulting from retinal ganglion cell (RGC) death is a leading cause of irreversible blindness. There are several areas of active research aimed at restoring retinal ganglion cells. One of them is endogenous repair. However, for this approach to work, we need to gain a better control of the developmental mechanisms

leading to RGC formation. In this study, we use ectopic overexpression of four specific transcription factors involved in ganglion cell specification and differentiation to bring about the direct conversion of ganglion cells from human pluripotent stem cells. If these newly differentiated neurons turn out to be truly bonafide ganglion cells, then the idea of generating new ganglion cells to improve the prognosis of retinal diseases will be better understood.

INTRODUCTION

Retinal lamination and cell types

In the retina, there are five main types of neuronal cells, which include photoreceptors, bipolar cells, horizontal cells, amacrine cells, and ganglion cells. In addition, there are three types of glial cells, including Müller glia, microglia, and astrocytes. The retina is structured in horizontal and vertical layers and is denoted by the cells that compose them. The photoreceptors, of which there are four main types (rods and blue, red and green sensitive cones), make up the outer nuclear layer (ONL) of the retina and serve as the primary site for the reception of vision forming light signals. Their axons extend towards the outer plexiform layer (OPL), where they form a synaptic triad with bipolar and horizontal cells. Bipolar cells in turn connect with RGCs in the inner plexiform layer (IPL) which finally send light impulses towards the brain. Amacrine and horizontal cells modulate these signals to enable a high degree of visual acuity (Masri, 2019).

There are many RGC subtypes. In the macaque retina, seventeen types of RGCs with unique morphologies have been identified via a process called "photofilling," where cells are labelled with rhodamine dextran. When the cells then are exposed to light, the dextran diffuses through the cell dendrites and reveals the morphology of the cell. The different types of RGCs are identified based on their unique stratification pattern and morphology. About 80% of RGC subtypes fall under three different categories, including midget, parasol, and small bistratified cells. These cells project to the lateral geniculate nucleus in the dorsal thalamus. The midget ganglion cell typically helps with encoding high resolution vision and red/green color vision while the parasol ganglion cell is better for motion detection. Generally, RGCs work in an "on/off" dichotomy. Most ganglion cell types, including the midget and parasol subtypes have

concentric receptive fields with an “on” center and an “off” surround, or an “off” center and an “on surround.” The “on” center RGCs become excited by an increase in light while the “off” center RGCs become excited by a decrease in light. Ultimately, the “on/off” system enables high contrast sensitivity and expedient transfer of information for changes in light stimuli (Schiller, 1986).

The remaining 20% of RGC subtypes are called widefield ganglion cells. Relative to the midget, parasol, and small bistratified cells, the widefield cells have a wider dendritic field. This widened dendritic field predominantly contributes to peripheral vision (Masri, 2019). The widefield ganglion cells are more heterogenous in nature but have a more dramatic dendritic reach. What is known is that some widefield RGCs respond to an onset and offset of light stimuli. Some widefield RGCs had a phasic response while others had a sustained response in the presence of light. Interestingly, it was also found that there was another subtype of widefield RGC that was both unresponsive to stationary stimuli and also inhibited by motion. This subtype of RGC is less well studied because of the difficulty involved in measuring the extent of their dendritic arbor in the IPL (Yamada, 2012). In the context of vision, it is known that various cell types serve specific purposes and are selectively tuned to recognize certain visual cues such as motion, size, direction, and color. If a certain signal is undetectable by the ganglion cells, it cannot be processed by the brain (Nelson, 2007). Having a heterogenous subtype of RGC like the widefield RGC enables a more fine-tuned visual system.

Eye development

Vertebrate eye development is the result of coordinated communication between the neuroepithelium, surface ectoderm, and extraocular mesenchyme. These layers themselves are influenced by neural crest and the mesoderm. From there, the optic vesicles are formed by the

invagination of the ventral forebrain. The distal section of the optic vesicles contacts the surface ectoderm and induces the formation of the lens placode. The lens placode and distal optic vesicle contact, causing the formation of a bilayered optic cup. The outer layer of the optic cup gives rise to the retinal pigment epithelium, while the inner layer gives rise to the neural retina. There is an additional layer between the inner and outer optic cup, which eventually leads to the development of key peripheral structures, including the iris epithelium and the ciliary body (Fuhrmann, 2010).

The primary components that make up the eye include the retina, retinal pigment epithelium (RPE), lens, iris, and cornea. The progenitors of the retina, RPE, and optic stalk make up the optic vesicle, which is the earliest morphogenic event required for eye formation. In order to induce neural plate induction, Bone Morphogenic Protein (BMP) signaling must be inhibited. Other factors involved in this early process include Wnts and Wnt inhibitors, Insulin-like Growth factors (IGF), and Fibroblast Growth Factors (FGF) (Giger, 2018).

There are numerous morphogens and growth factors involved in early eye development. Cyclops and Sonic hedgehog (Shh) are both involved in the splitting of the eye field as well as the proximo-distal patterning of the optic vesicles (Adler, 2007; Albert, 2003). Sonic hedgehog, Fibroblast Growth Factors, Activin, Bone Morphogenic Protein 7, and retinoic acid have all been implicated in the process of optic vesicle patterning. Retinoic acid has also been shown to be involved in the invagination of the optic vesicle into an optic cup (Adler, 2007). Finally, the morphogens involved in the antero-posterior and dorso-ventral patterning in the optic cup include Nodal, FGFs, Shh, BMP, Retinoic Acid, Ventroptin, Follistatin, Chordin, Noggin, and DAN domain family members (Adler, 2007; Albert, 2003).

Transcription factor involvement in eye development

Cells in the early eye field show expression of a set of eye field transcription factors, including Pax6, Rax, Six3, and Lhx2. These factors are required for both eye development and implicated in forebrain development, which makes it somewhat difficult to specifically narrow down all of the upstream pathways needed to establish the eye field (Heavner, 2012). Pax6 is widely considered to be a master regulator of eye development, and Sonic Hedgehog signaling has been found to regulate the expression of the Pax genes (Isenmann, 2003). The expression of Six3 precedes Pax6 expression and actually serves to activate Pax6 transcription. BMP4 signaling activates SOX2 but not Pax6, while Bone Morphogenic Protein 7 may activate Pax6 (Heavner, 2012).

There are multiple transcription factors that govern RGC development. These include Neurogenin-2 (NGN2), Atonal homolog 7 (ATOH7), Islet-1 (ISL1), Neurod-1, and Achaete-scute homolog 1 (ASCL1) which together regulate neurogenesis by influencing cell survival, cell cycle exit, and differentiation (Hufnagel, 2011; Luo, 2019). Additionally, the transcription factor POU4F2 (also referred to as BRN3B) has been shown to promote the differentiation of retinal progenitors into RGCs (Xiang, 2011). Another set of transcription factors involved in RGC differentiation are the Sry-related high mobility box (Sox) superfamily of genes. More specifically, the SoxC genes, which include Sox4, Sox11, and Sox12, influence the direction of axonal growth and RGC differentiation (Chang, 2017).

While many genes regulate RGC development, a number are implicated in RGC development. First, neurogenin-2 plays an important role in early neural development and functions before the formation of specific neural lineages. In stem cells, NGN2 alone has been shown to rapidly convert iPSCs and embryonic stem cells to neurons. After four days, the cells took on a neuronal morphology and were homogeneous in function and transcriptional profile

(Wang, 2017; Busskamp, 2014). Additionally, it has been shown in chick and mouse that ATOH7 coordinates with NGN2 to differentiate into immature RGCs from cultured RPE cells and these transcription factors are activated at an early stage in cells (Hufnagel, 2010). While the mechanism is unknown, NGN2 has been shown to directly activate the ATOH7 promoter. ATOH7 in turn activates other downstream transcription factors, including ISL1 and BRN3B, which then leads to RGC fate determination (Wu, 2015). In mice, the combination of ATOH7 and BRN3B together is sufficient to reprogram Müller glia to RGCs while either transcription factor alone had a limited capacity to do so (Xiao, 2019). The ISL1 gene encodes a LIM-homeodomain transcription factor that has a significant role in the specification, differentiation and maintenance of RGCs, horizontal cells, and amacrine cells in a wide variety of species, including reptiles, fish, birds, and mammals (Luo, 2019). In mice, conditional inactivation of ISL1 leads to optic nerve hypoplasia and 70% RGC cell loss. Moreover, this loss of ISL1 further resulted in delayed RGC axon elongation and errors in RGC axon pathfinding, further demonstrating its crucial role in RGC development (Xiang, 2011). While ISL1 and BRN3B are both required for RGC development, the mechanism of coordination between these genes is unclear. Yet, it is known that they co-occupy the promoters to a multitude of important genes and signaling pathways. One of the pathways that BRN3B activates is the Shh pathway. It has also been suggested that BRN3B acts to repress other groups of genes involved in non-RGC development (Xiang, 2011). The final three genes of note compose the SoxC family and include Sox4, Sox11, and Sox12. It has been demonstrated that the loss of Sox4 and Sox11 during early retinal development resulted in a complete lack of RGC presence as well as the loss of optic nerve formation (Jiang, 2013). The SoxC family of genes also antagonizes the transcription factor Hes5 which suppresses RGC differentiation. The SoxC genes also control contralateral but

not ipsilateral RGC differentiation (Chang, 2017). **Figure 1** illustrates the relationship between these transcription factors and their role in RGC differentiation.

Endogenous regeneration

Endogenous regeneration involves utilizing the innate self-repair potential from an organism's own tissue. Endogenous stem cells are adult stem cells with tissue specificity and a capacity for self-renewal and differentiation. Most mammals have a highly limited capacity for scar-free healing and regeneration, which is largely limited to the earliest stages of life (Xia, 2018). Yet, many non-mammalian vertebrates maintain the ability for scar-free healing and regeneration throughout their entire life. For instance, adult zebrafish have been shown to regenerate various organs and tissues after injury (Marques, 2019). The regenerative potential of the adult zebrafish is very well studied, and it has been shown that besides the retina, zebrafish are able to regenerate their fins, spinal cord, heart, and kidney (Beffagna, 2019). Here, the goal is to utilize endogenous stem cells to recapitulate the regeneration potential observed in other non-mammalian vertebrates.

Many non-mammalian species demonstrate robust regeneration potential. For example, the zebrafish is a benchmark species for studying regeneration due to its experimental accessibility (Marques, 2019). In the retina, they can regenerate a damaged retina by utilizing existing Müller glial (MG) cells (Xiao, 2019) which following an injury signal, can undergo cell division to produce a progenitor cell population capable of differentiating into the major cells that compose the retina (Wan, 2016). Additionally, in the xenopus, it has been shown that RPE cells have the potential to regenerate an injured retina via transdifferentiation (Vergara, 2009).

Signaling pathways in endogenous regeneration

Although the mechanisms are not entirely understood, there are a number of transcription factors that participate in endogenous regeneration. Following injury, many proneural transcription factors are upregulated (Madelaine, 2017). These include achaete-schute homolog 1a (Ascl1a), which induces the expression of lin-28, a pluripotency promoting mRNA binding protein. Thus, ASCL1 converts existing Müller cells into a more primitive stem-like state. Additionally, in zebrafish, the transcription factors sex-determining region Y-box 2 (SOX2) and ATOH7 have shown increased expression in MG as a response to injury (Gorsuch, 2017; Madelaine, 2017). Both are typically expressed in neural progenitors and early stage retinas. This cascade of signaling starts with SOX2 inducing expression of Ascl1a and ATOH7, both of which subsequently lead to the expression of lin-28 (Madelaine, 2017).

Another signaling pathway implicated in regeneration is the Hippo pathway. When the Hippo pathway functions normally, it inhibits a number of factors implicated in regeneration. It has also been shown that inactivation of the Hippo signaling pathway enables injured cells to revert to a progenitor-like state (Rueda, 2019). This pathway was originally established as an organ size regulator in drosophila but is highly conserved in mammals as well. The Hippo pathway begins with Mammalian STE20-Like Protein Kinase 1/2 (MST1/2) and Mitogen-Activated Protein Kinase Kinase Kinase Kinase (MAP4K), both phosphorylating Large Tumor Suppressor Kinase 1/2 (LATS1/2). Activation of LATS1/2 leads to the phosphorylation of Yes Associated Protein (YAP) and Transcriptional Co-Activator with PDZ-Binding Motif (TAZ), which leads to their inactivation. Phosphorylated YAP/TAZ does not translocate to the nucleus. When the Hippo pathway is downregulated, the unphosphorylated YAP/TAZ moves to the nucleus and begins transcription by interacting with the four TEA Domain transcription factors (TEAD 1-4). YAP is highly expressed in embryonic stem cells but upon cell differentiation

becomes inactivated. YAP levels are high during early embryonic development but drop after birth. Yet, YAP/TAZ levels quickly rise again upon tissue injury which leads to the expansion of progenitor cells and the dedifferentiation of somatic cells (Wang, 2017). An overview of the Hippo signaling pathway is delineated in **Figure 2**. Since it is known that activation of the Hippo pathway leads to the inactivation of YAP/TAZ, which themselves are important factors for regeneration, it is clear that the Hippo pathway plays an inhibitory role in cell reprogramming and regeneration. Typically, the Hippo pathway blocks persistent cell cycle re-entry following injury. Yet, it has been shown that when YAP is made unresponsive to Hippo signaling, injured cells are reprogrammed to a progenitor-like state (Rueda, 2019).

One of the most important pathways involved in mammalian regeneration is the Wnt signaling pathway. Of the overarching Wnt signaling umbrella, there is a canonical Wnt signaling pathway which is a β-catenin dependent pathway, and a non-canonical pathway which itself is further divided into the Wnt/Ca2+ pathway and the Planar Cell Polarity pathway (Komiya, 2008). The canonical pathway, which is a β-catenin dependent, seems to be the specific Wnt pathway that is most applicable to regeneration. The mechanism of action in the canonical Wnt signaling pathway leads to the accumulation of β-catenin which subsequently is translocated to the nucleus where it leads to transcription. In the absence of Wnt, a β-catenin destruction complex composed of five factors: Axin, protein phosphatase 2A (PP2A), adenomatosis polyposis coli (APC), casein kinase 1α, (CK1α), and glycogen synthase kinase 3 (GSK3), serves to degrade the cytoplasmic β-catenin. Once Wnt is present, it binds to a seven-transmembrane receptor complex including the Frizzled receptor (FZD) and low-density lipoprotein receptor-related protein 5/6 (LRP5/6). The binding of Wnt to this receptor complex causes Axin to bind to the LRP5/6 receptor and disrupts the β-catenin destruction complex. This

leads to a positive feedback loop and a subsequent accumulation of a β-catenin in the cytoplasm. Additionally, the binding of Axin has been shown to activate the phosphoprotein Dishevelled (Dsh), which is also activated by casein kinase 1α. Dsh inhibits the activity of GSK3 which further leads to an accumulation of β-catenin. The accumulated Wnt in the cytoplasm eventually travels to the nucleus by "piggybacking" off of other factors that similarly translocate into the nucleus. Once in the nucleus, Wnt complexes with T-cell factor/lymphoid enhancer factor (TCF/LEF) and mediates transcription. The canonical Wnt signaling pathway is illustrated in **Figure 3**. While it has been established that the non-canonical pathway has been involved in certain inflammatory diseases, the role of that pathway is still unclear. It has been shown that Wnt signaling is not only crucial in species with robust regenerative capabilities such as zebrafish and salamanders but also plays a role in mammalian organs and tissues that have a limited regenerative capacity. Additionally, when Wnt signaling is decreased, so does the regenerative ability of the organism. The disruption of Wnt signaling leads to decreased recruitment of stem and progenitor cells to the injury site. For instance, in zebrafish, when Wnt signaling is blocked following a dorsal fin injury, the fin is unable to regenerate normally (Whyte, 2012).

The Bone Morphogenic Protein signaling pathway is also important for embryogenesis and regeneration. The BMP molecules are part of the Transforming Growth Factor β (TGF- β) protein superfamily. Like the Wnt signaling pathway, BMP signaling has both canonical and non-canonical pathways that have different mechanisms. The canonical pathway begins with BMP binding to receptors on the cell surface. These receptors form a complex of type I and type II dimers, which are serine/threonine kinase receptors. Upon binding of BMP, these heterotetrameric complexes phosphorylate a downstream protein family called the receptor-

regulated Smads (R-Smads). The specific R-Smads that are associated with the canonical BMP signaling pathway are Smad1, Smad5, and Smad8. From there, the R-Smads group with a co-mediator protein called Smad4 which then moves to the nucleus and acts as a transcription factor. Importantly, there are many proteins that serve as BMP antagonists, including noggin and chordin (Wang, 2014). In various studies, it has been shown that noggin treatment in neonatal mice causes a decrease in regenerative ability (Costamagna, 2016). It has been suggested that BMP treatment leads to the initiation of a reprogramming event that leads to an increase in regeneration (Yu, 2010).

Fibroblast Growth Factors facilitate regeneration by controlling cell differentiation, survival, movement, and growth. The mechanism of action for most FGFs is a binding to four tyrosine kinase receptors, called FGFR1-4, located along the cell membrane. Upon binding to their respective receptors, the FGFs cause the activation of multiple signaling pathways. The most relevant is the Ras-Erk1/2 pathway, but other pathways such as the STAT1/3/5 and phosphatidylinositol 3-kinase/AKT pathway play a role as well. The FGFs work in coordination with other signaling pathways such as the Wnt pathway to increase the regenerative capacity of many organisms (Maddaluno, 2017).

Finally, the Hedgehog signaling pathway is a crucial development regulator and is required for cell differentiation. The most well-researched hedgehog homolog is Sonic hedgehog (Shh). The canonical Shh signaling mechanism begins with the binding of Shh to the 12-transmembrane protein named Patched (Ptch1), which leads to its inactivation. Ptch1 usually represses smoothened (Smo) activity so when Ptch1 is inactivated, Smo activity increases. An increase of Smo levels leads to the activation of multiple signaling cascades, eventually resulting in an upregulation of glioma-associated oncogene homolog (Gli) proteins and its subsequent

translocation to the nucleus, which leads to transcription. This signaling pathway is presented in **Figure 4**. The presence of Gli in the nucleus also causes changes to the Wnt signaling pathway. The crosstalk between the Shh pathway and the Wnt pathway is dynamic. In Wnt signaling, β-catenin is inhibited by Gli, while TCF/LEF upregulates Gli (Carballo, 2018). The dynamic crosstalk between Shh and Wnt signaling is shown in **Figure 5**. It has been demonstrated that in axolotls, Shh signaling controlled dorsoventral patterning and was required for tail regeneration. When Shh signaling was restricted, axolotl tail regeneration was strongly inhibited (Schnapp, 2005).

Stem cells and differentiation potential

Most mammals lose much of their cell and tissue regeneration potential after their earliest stages of development (Xia, 2018). Yet, it has been shown that cells that have already differentiated still have the potential to be reprogrammed to a pluripotent state by introducing expression of specific transcription factors. These cells, named induced pluripotent stem cells (iPSCs), were able to be reprogrammed from somatic cells via introduction of four transcription factors, Oct3/4, SOX2, Klf4, and c-Myc. (Takahashi, 2006; De Los Angeles, 2015).

Stem cells are the general classification for cells that have the ability to self-renew and differentiate into many different cell types. Within the stem cell umbrella, there are different levels of potency. Unipotent or multipotent stem cells maintain their ability to self-renew yet have very limited developmental capacity with regard to lineage. Pluripotent stem cells (PSC) can regenerate any cell in the body, including tissue from all three germ layers found in a developing embryo including the ectoderm, the mesoderm, and the endoderm. Yet, they are unable to contribute to the trophoblast layers of the placenta or extra-embryonic tissue. A

totipotent stem cell has all of the differentiation potential of a PSC but is also able to differentiate to any of the tissues required for embryonic development (De Los Angeles, 2015).

While stem cells have the ability to differentiate into other cell types, somatic cells have the potential to convert directly into another cell type in a process called direct cell reprogramming, or transdifferentiation. During the process of transdifferentiation, a somatic cell is able to transition into another cell type without entering an induced pluripotent state (Grath, 2019). Transdifferentiation provides the potential for an existing somatic cell to differentiate directly to another cell type, enabling potential cell therapies and non-surgical treatments that were previously not possible.

Clustered regularly interspaced short palindromic repeats (CRISPR) gene editing

CRISPR, or clustered regularly interspaced short palindromic repeats, is a tool for genome editing that involves two primary components – a guide RNA (gRNA) and a Cas9 endonuclease (Addgene, 2017). The gRNA is itself made up of two RNAs, the crRNA, which identifies the genomic target for Cas9, and TracrRNA, which serves as a scaffold to link the crRNA to the Cas9 and enables facilitation and processing of mature crRNA from pre-crRNA. The gRNA contains the target sequence required to direct the Cas9 protein to a specific locus in the genome as well as the scaffolding required for Cas9 to bind (Addgene, 2017). The Cas9 protein, or CRISPR Associated Protein 9, binds to the target DNA when in the presence of gRNA when the target is 5' to the protospacer adjacent motif (PAM) sequence. The PAM sequence is a short DNA sequence that provides the binding signal for Cas9. In order for the double-stranded DNA to be cut, it must contain a PAM sequence 3' of the target site (Addgene 2017).

An alternative to Cas9 is Cpf1/Cas12a. Relative to Cas9, Cpf1 cleaves DNA in a staggered pattern and only requires one RNA instead of two. This staggered cleaving pattern

enables directional gene transfer and could be helpful when targeting non-dividing cells, which are traditionally difficult to modify via homology-directed repair (HDR). Utilization of Cpf1 also expands the potential number of CRISPR target sites to regions in the genome that are AT-rich and lack the specific PAM sequences used by Cas9 (Addgene, 2017).

Vision disorders and treatmentsc

Glaucoma is the second highest cause of blindness in people today and is caused by increased intraocular pressure leading to retinal ganglion cell death (Quigley, 1999; Levin, 2002). Similarly, retinal ischemia is the result of an interruption to the retinal circulation and causes irreversible RGC death in minutes (Levin, 2002). In both of these cases, finding a way to generate new RGCs could be a potential pathway to restore vision.

Glaucoma is a type of optic neuropathy defined by a continual loss of RGCs. It impacts an excess of over 70 million people globally and causes irreversible blindness. RGC death due to an increase in intraocular pressure is the primary cause of glaucoma.

Currently, the top goal for treating glaucoma involves maintaining a high quality of life for those affected by slowing the progression of the disease. The main method for improving symptoms caused by this disease is by finding a way to decrease intraocular pressure. Yet, the problem remains that if this disease is not diagnosed quickly, there is a real chance that irreversible RGC death has already occurred (Weinreb, 2014).

Transdifferentiation of neuronal cells from human pluripotent stem cells

The focus of this study offers an alternative method for treating diseases like glaucoma by utilizing the process of endogenous regeneration to regenerate ganglion cells that were previously considered irreversibly lost. My hypothesis was that if specific transcription factors involved in RGC specification and differentiation were ectopically overexpressed, then the level

of endogenous regeneration observed in species such as zebrafish could be recapitulated in humans to generate new RGCs. Our results show that the overexpression of four specific transcription factors, NEUROG2, ATOH7, ISL1, and BRN3B caused the generation of neurons with RGC-like expression. The results of this study will aid in better understanding of how overexpression of transcription factors can cause cells to undergo direct conversion to recapitulate the process of endogenous regeneration. It will also explore the relationship between the primary genes involved in RGC generation.

RESULTS AND DISCUSSION

Characterization of human stem cell-derived retinal organoids

The process of generating 3D retinal organoids was done by gravity assisted forced aggregation of dissociated undifferentiated stem cells which under defined cell culture conditions spontaneously form laminar organized retinas. We validated that stem cell-based retinal organoids encoding a SIX6-eGFP / Brn3b-tdTomato dual reporter retain their ability to form RGCs as well as a laminated retinal structure. A visual schematic outlining the timeline for organoid development can be found in **Figure 6**. These organoids began as a group of 125 dissociated stem cells and were kept in hypoxia until day 5, after which time they were transitioned to normoxia. The small molecule inhibitors of Wnt or activators of Smoothened were also used during early and late time periods to promote optic vesicle formation. During the first seven days of differentiation we observed that the morphology of aggregates that originally appeared small and translucent quickly darkened in color as it grew in size. A summary of the first week of morphological development can be seen in **Figure 7**. After a week they started forming optic vesicles. Finally, these vesicles matured and took on a retina cup morphology. I verified that these structures acquired eyefield characteristics by documenting the appearance of *SIX6*-eGFP which is expressed in optic vesicles as well as hypothalamic structures (Conte, 2005). SIX6-eGFP can typically be first seen on day 10, while Brn3b-tdTomato can first be visualized in RGCs on day 25. Bonafide retinas were thus verified by the onset of BRN3B-tdTomato expression. **Figure 8-I** shows the dual reporter in the 3D organoids as well as how BRN3B expression increased between the span of day 27 to day 32.

Design of a multiplexed transgene construct for RGC induction

The long-term goal of this project was to create a tool that could cause stem cells to differentiate to RGCs and cause other cell types such as the Müller cells to transdifferentiate into RGCs. The short-term goal of this project as well as the focus of this thesis, was to generate the molecular tools necessary to drive multiplexed transgene expression in an inducible fashion. The plasmid construct used to induce RGCs contained four RGC promoting genes, NGN2, ATOH7, ISL1, and BRN3B (NAIB) each separated by a P2A sequence enabling polycistronic expression of genes via ribosome skipping. Each gene in the NAIB cassette plays an important role in RGC specification. NGN2 is primarily for early neural induction while ATOH7 and ISL1 are needed for RGC commitment and BRN3B is used to cause RGC differentiation (Hufnagel, 2010; Wu, 2015). The NAIB cassette is under the control of a third-generation tetracycline (TET) activated response element (3G -TRE) and a constitutively expressed reverse tetracycline trans-activating sequence (rtTA). A constitutively active TagBFP2 under a chicken beta-actin hybrid (Cbh) promoter was used to visualize gene integration and was co-expressed with a zeocin selectable marker to remove unmodified cells, thus allowing us to achieve a pure population of gene integrated cells.

The primary components of the cassette include four transcription factors that have been heavily implicated in the process of RGC formation. The first gene was NGN2, which was amplified from complementary DNA (cDNA). The cDNA came from day 18 differentiated optic vesicles. Total RNA, including mRNA, was extracted from these optic vesicles and reverse transcribed to make cDNA. Using cDNA as the polymerase chain reaction (PCR) template was ideal because cDNA produces only exons and no introns. Once PCR amplified, it was cloned into a separately PCR amplified plasmid DNA backbone by Gibson assembly. Gibson assembly is an isothermal reaction that utilizes 5’ exonuclease, DNA polymerase, and DNA ligase

enzymes to join DNA fragments with overlapping homology. Once the Gibson assembly was complete, I restriction enzyme digested the reaction product with a methylation specific DPN1 enzyme which degraded the original plasmid template, ensuring that all that is left is the desired new DNA product. Once NGN2 was in the new DNA backbone, it served as the template for the addition of the next gene, ATOH7.

Next we amplified the ATOH7 gene from genomic DNA (gDNA), which was possible because ATOH7 does not contain any introns. The ATOH7 coding sequence has a 70% GC content and initial attempts to amplify this fragment failed. GC-rich genes are difficult to amplify because they are more stable than GC-poor structures and form secondary hairpin structures. The GC content of ATOH7, as well as other GC-rich genes in the NAIB cassette are shown in **Figure 9**. To overcome the challenge of amplifying GC-rich genes, the annealing temperature of the PCR reaction was increased from 65□ to 72□ and 2% Dimethyl sulfoxide (DMSO) was added to the reaction mix. DMSO increases the heat sensitivity of GC-rich areas and also reduces the primer melting temperature (Tm). The tradeoff is that DMSO increases the likelihood of base mispairing, leading to an increased chance of mutations. Another issue that had to be overcome when amplifying ATOH7 was the overlap with the repetitive P2A sequences in the plasmid. P2A repeats are important because they enable ribosome skipping during translation and thus give the cassette the ability to express multiple genes separately and at the same time by generating individual proteins from a single mRNA transcript (Daniels, 2014). The problem with the presence of P2A sequences when amplifying via PCR is that there are multiple sequences in the template that have a high level of similarity to one another. Single base pair mutations were introduced to the sequences in order to create new versions that were identical at the protein level but differed significantly at the nucleic acid level. This allowed for PCR and Gibson assembly,

even when these regions were shared by multiple P2A sequences. The exact sequences of these P2A variants is illustrated in **Figure 10B**. While this approach improved the efficiency of Gibson assembly, the P2A repeats were still problematic as the multi-cistronic chain became more complex. To solve this problem, a 2-step PCR approach was used. First, the PCR shell was amplified to have no overlap with the P2A repeats on either end. While this enables facile amplification, this step alone would make a successful Gibson assembly impossible as there is no homology with the ATOH7 insert. The solution was in the ATOH7 insert amplification. In this insert, a first set of primers was used that amplified through part of the P2A repeats. After this first step, the PCR product was purified and concentrated, then put through another reaction with new primers that elongated the PCR product overhangs to overlap with the DNA backbone. These overhangs are typically at least 20 base pairs long and are required for Gibson assembly. An outline of the 2-step PCR strategy and primer design can be seen in **Figure 11A-D**.

ISL1 and BRN3B were subsequently amplified by the same approach as above. Once the PCR reaction was complete, agarose gel electrophoresis was carried out to confirm the presence of the desired product. As more of the transcription factors that make up the NAIB cassette were added to the DNA backbone, we verified incorporation of each gene fragment by PCR with a common set of oligonucleotide primers that give PCR products with increasing size based on its cargo. **Figure 10A&C** shows the addition of each subsequent gene in the NAIB cassette increased the molecular weight of the band visualized on the agarose gel. During the initial amplification of PCR products for cloning, multiple bands were often observed during agarose gel electrophoresis instead of the single expected band. The presence of multiple bands is problematic since these superfluous bands represent a DNA fragment with overlapping ends as the desired product and could lead to decreased efficiency during Gibson assembly. To eliminate

unwanted bands, I gel extracted the desired band after visualizing the DNA with SYBR-SAFE by manually excising the correct band with a razor blade under blue light, followed by gel extraction using a Zymo-5 cleanup column. Once the fragments were successfully isolated, Gibson assembly was once again used to join them with the rest of the cassette. In order to ensure that the actual Gibson product matched the expected sequence, Sanger sequencing was used to verify the areas surrounding the newly inserted gene.

As each gene was sequentially integrated into the growing plasmid, they were transformed into bacteria. The plasmid backbone has an ampicillin antibiotic resistance gene, which enables antibiotic selection on lysogeny broth (LB) carbenicillin plates. When cloning repetitive sequences, such as those including P2A repeats one can experience unwanted spurious recombination resulting in gene deletion. To mitigate the odds of this happening, STBL competent cells from New England Biolabs (NEB) were grown at 30□ to reduce the likelihood of this happening. The bacteria were grown overnight in LB with carbenicillin for a total volume of 50 ml. The bacteria were grown to an OD of 2.5 and purified using endotoxin free Midiprep to obtain transfection grade plasmid DNA. To verify the sequence integrity of plasmids I used sanger sequencing and performed DNA sequence alignments with the Geneious bioinformatics suite to the expected sequences to rule out unwanted mutagenesis. Sequencing data can be found on **Figure 12**. It was important that the sequences had overlap between one another to minimize ambiguous reads and ensure that there was a consensus between multiple sequencing files.

In addition to the four genes, this cassette also has a few characteristics that give it more control and specificity when put into cells. The four genes are under the control of a tetracycline inducible promoter which is only activated in the presence of tetracycline/doxycycline. This cassette also has an inducible mTagBFP2 reporter which will cause the cells to turn blue once the

cassette has been activated. In addition to the four genes, there is an additional cassette preceding the NAIB cassette, which contains a zeocin antibiotic resistance gene and an additional mTagBFP2-nls which is constitutively expressed and produces a blue nuclear signal. This cassette is under the control of a Cbh constitutive promoter. The organization of this cassette can be visualized in **Figure 13**. The role of this cassette is to provide the cells which integrate the genetic cargo with resistance to the selectable marker zeocin such that when the cells are treated with this antibiotic, only the cells that have successfully taken up the construct survive, enabling the selection of pure modified cells.

NAIB construct transfection and overexpression for RGC generation

Once the DNA construct was complete with the successful addition of the NAIB cassette, the plasmid was transiently transfected into a human induced pluripotent stem cell line (IMR90.4) in order to demonstrate transdifferentiation. In a transient transfection, the NAIB cassette enters the cell but is not stably integrated into the genome. Briefly, when the stem cell colonies were at a high density, they were single cell passaged with accutase. Approximately 100,000 to 200,000 cells were used per transfection. Multiple transfections were carried out in different conditions. After two days of doxycycline treatment, some neurons were apparent, but they were quickly overrun by stem cells. Representative images from this transient transfection can be observed in **Figure 14A-C**. Next, another transfection was carried out where the NAIB cassette was co-transfected with the Cpf1 expressing pY026 plasmid which co-expresses a Cpf1 enzyme and a CLYBL targeting guide sequence. This was necessary since the cells already contained a Tet-inducible Cas9 and rtTA and the addition of doxy to the culture would cause premature activation of NAIB cassette, eliminating the possibility of obtaining a stable stem cell line. The cell line we chose for introduction of the NAIB cassette was a SIX6-p2a-GFP and

Brn3b-p2a-tdTomato dual reporter IMR90 iPSC line which would allow us to visualize cells in real-time as they convert to RGCs. Verification of stable integrated cells was accomplished by a constitutive expressed mTagBFP2. Cells were treated with zeocin, ensuring that all of the cells that did not integrate NAIB died off, resulting in a mostly pure population of blue cells. Following selection of modified cells, I carried out doxycycline induction to trigger neural differentiation. Following treatment with doxycycline (1 μg/ml), a shift towards a neuronal morphology was evident after only two days (**Figure 15**). In addition to the obvious morphological changes there were also other neuronal changes that were observed. BRN3B-tdTomato+ cells were observed and exhibited a classic neuronal appearance with long neurites (see arrows). One interesting observation was that the mTagBFP2 in the doxycycline treated sample was not as intense as in the non-doxycycline treated sample. One possible explanation is that as the cells differentiate, the mTagBFP2 signal is silenced. Regardless, a faint mTagBFP2 signal was still visible in the differentiated cells. Importantly, the cells that expressed mTagBFP2 and demonstrated a morphological change had colocalization of both SIX6-eGFP and BRN3B-tdTomato, while the non-doxycycline treated cells only expressed mTagBFP2 but not SIX6-eGFP or BRN3B-tdTomato **(Figure 15 B-D, F-H)**.

This project had other experiments planned that were severely impacted by the COVID-19 pandemic that would further improve the rigor of this study. Future experiments include a comparative transfection where each gene included in the NAIB cassette is transfected into cells individually to compare how each gene impacts RGC differentiation relative to when the genes are used together. Moreover, the addition of certain growth factors such as ciliary neurotrophic factor (CNTF) and brain-derived neurotrophic factor (BDNF) offer the potential for improving the long-term survivability of these differentiated RGCs (Zhang, 2005). Additionally, I wanted to

perform a western blot and NGS on the cells that expressed the NAIB cassette to validate the overexpression of the transgenes and efficient poly-cistronic expression of individual NAIB genes.

Materials and Methods

Cells. IMR90.4 iPSCs and WA09 ES (both from WiCell) and EP1.1 cell (Donald Zack; JHU) were used for the following study. Cells were routinely tested for mycoplasma by PCR. PSCs were used with approval from the UC San Diego Institutional Review Board.

Single-cell passage and maintenance of PSCs. Stem cells were maintained antibiotic free on 1% (vol/vol) Matrigel(MG)-GFR™ (#354230; BD Biosciences) extracellular matrix (ECM) coated dishes at 37°C under hypoxic conditions (10% CO_2/5%O_2) in mTeSR1 (Stem Cell Technologies) as previously described (40-43). Cells were passaged every 4-6 days, with Accutase (#A6964; Sigma) for 10-12 minutes, dissociated into single cells, quenched with mTeSR1 plus 5μM blebbistatin (B; #B0560; Sigma), pelleted at 80 x *g* for 5 minutes, resuspended in mTeSR1+B and plated at 2,000 cells per single well of a 12-well plate. After 48 hours, cells were fed with mTeSR alone.

Cloning. See **Table 1** (Table 1) for a complete list of oligos.

Plasmid preparation for transfection. For routine growth of plasmids, we used chemically competent Stable *E. coli* cells (#C3040I; NEB). DNA for transfection was prepared using the endotoxin-free grade Plasmid Plus Maxi Kit (#12963; Qiagen) or ZymoPURE Plasmid Midiprep Kits (#11-550; Zymo). Purified plasmid was resolved by agarose gel electrophoresis to rule out RNA or genomic DNA contamination. Plasmids used for quantitative studies of HDR efficiency were never thawed more than 3 times to prevent unwanted degradation of plasmids. PureLink RNA Mini Kit (#12183020; Thermo Fisher Scientific) was used to purify total RNA to be used for subsequent cDNA synthesis.

Constructs for generating Tet-inducible HF-iCas9 Cells. The laboratory previously created inducible Cas9 PSCs to facilitate gene-editing. The method is briefly described here. To create

HF-ieCas9 cells we targeted the AAVS1 safe harbor site inserting a reverse tetracycline-controlled trans-activator (rtTA) expression cassette at one allele and a 3G-TET regulated eSpCas9 at the other. When bound to doxycycline, constitutively expressed rtTA binds to the Tet operator and ieCas9 expression is induced. The rtTA coding sequence was provided by AAVS1-Neo-M2-rtTA plasmid (Addgene; #60843) whereas the ieSpCas9 coding sequence was amplified from eSpCas9(1.1)(Addgene #71814) (6) and cloned into the AAVS1-puro-Cas9 donor (Addgene #58409) . Briefly, the AAVS1 donor shell was amplified with Phusion Polymerase (#F548L; Invitrogen) using the oligos Cas9backbone_F and Rev and the ieSpCas9 insert was amplified using the oligos Cas9insert_for and Cas9insert_rev **(Table 1)**. PCR products were cleaned using DNA Clean and Concentrator-5 columns (#D4014; Zymo Research) and donor and insert PCR products were fused together using Gibson assembly reagents (#E2611S; NEB), followed by overnight digestion with Dpn1 enzyme (#R0176L; NEB) to remove parental template DNA. The Gibson product was transformed into chemically competent Stable *E. coli* cells and colonies were miniprepped and verified by Sanger sequencing. For the AAaVS1 targeting, phosphorylated an oligo duplex of the AAVS1_esp_T1 forward and reverse oligos were ligated into BbsI cut pSpCas9(BB)-2A-puro (PX459) V2.0 backbone (Addgene #62988) using Quick ligase (NEB according to the manufacturer's specifications).

Reporter cells as a backbone. The cell line background used for this study was previously made by other lab members. Briefly a **SIX6-p2a-eGFP IMR90 iPSC line** was made using the following approach. The *SIX6* gene was targeted by amplifying a 1,311 base pair donor fragment (657 left homology arm and 654 base right homology arm). Immediately before the *SIX6* stop site, a p2a-H2B-eGFP cassette was inserted in-frame. A similar approach was taken to generate a **BRN3B-p2a-tdTomato** reporter. Both donors were electroporated into stem cells and stably integrated into

the genome via CRISPR-Cas9 gene editing.

Donor plasmids for transdifferentiation. Previously, a custom mini-circle compatible hybrid plasmid was constructed with a pUC origin of replication, ampicillin resistance gene, a docking site for the DNA donor fragment and a U6-gRNA-scaffold cassette. AttB and attP integrase recombination sites were introduced flanking this cassette for minicircle plasmid production and 2x SceI endonuclease sites introduced outside of this cassette for degradation of parental plasmid after mini-circle induction. ***NAIB* construct.** The NAIB construct was made by amplifying four genes (NGN2, ATOH7, ISL1 and BRN3B) from cDNAs from day 18 optic vesicles and gDNA. NGN2, ISL1, and BRN3B were all amplified from cDNA while ATOH7 was amplified from gDNA. When preparing cDNA, total RNA was extracted from differentiated organoids and reverse transcribed in a 20µl reaction using Superscript IV reverse transcriptase according to manufactures recommendations. Once the cDNA was prepared, it was used as the template for PCR amplification using Phusion Flash High-Fidelity PCR Master Mix (#F548s; Thermo Fisher Scientific). After each gene was amplified, it was run on a 1% agarose gel to confirm that the PCR product was a clean band at the desired size. Once the PCR product was confirmed to be the correct size, the PCR product was purified with the DNA Clean & Concentrator-5 (#D4013; Zymo Research). Following DNA purification, the genes were cloned into a linearized backbone (from above) and Gibson assembled using 20-30 base pair overlap with HiFi DNA Assembly Mastermix (#E2621S; NEB). The plasmid was then digested using Dpn1 enzyme (#R0176L; NEB).

Directed differentiation. Optic vesicles were generated as previously described (Wahlin et al. 2017) with minor modifications. Cell culture medium used for differentiation was as follows: BE6.2-NIM (B27 + E6 at 2X concentration) (neural induction medium) consists of DMEM (#11965; Invitrogen) supplemented with 1% B27 vitamin A (-) (#12587010; Invitrogen) and 2X

E6 supplement (38.8 mg/L insulin (#11376497001; Roche), +128mg/L L-ascorbic acid (#A8960; Sigma), 28µg/L selenium (#S5261; Sigma), 21.4 mg/L transferrin (#T0665; Sigma) and 38.8 mg/L NaHCO3). LTR (Long-Term Retina) medium was a 3:1 mix of DMEM:F12 (#11965, #11765; Invitrogen) supplemented with 1% B27 (#17504044; Invitrogen), 10% heat inactivated qualified-grade FBS (#16140071; Invitrogen), 1mM pyruvate (#11360; Invitrogen), 1xNEAA (#11140; Invitrogen), 1xGlutamax (#35050061; Invitrogen) and 1mM taurine (#T-8691; Sigma). For optic vesicle induction, PSCs maintained in mTeSR1 were used to initiate serum-free embryoid body forced aggregates. Stem cells were passaged with a longer Accutase incubation for 12 minutes and 1,000 cells in 50µl of mTeSR1+B were seeded per well into polystyrene 96-well U-bottom plates (#650180; Greiner). Aggregates were transitioned to BE6.2 medium by adding 50µl+2% MG on day 1 and 1% MG each day thereafter. On days 4-8, a 50% medium exchange (100 µl) was performed daily and every other day thereafter. Medium contained 1% (v/v) MG and 3µM of IWR-1e (a WNT inhibitor and AXIN2 stabilizer; #681669; EMD Millipore) from days 1-6. For long term maintenance, vesicles were transferred at day 10 to 15ml conical tubes, rinsed 3 times in HBSS, and resuspended in BE6.2+300nM Smoothened agonist (SAG; #566660; EMD Millipore) from days 10-12 to enhance retinal induction then LTR+SAG from days 12-18. For experiments longer than 16 days, we used sharpened tungsten needles to excise optic vesicles to prevent overgrowth and necrosis. Excision was typically carried out from days 10-12. To increase survival and differentiation, 500nM all-trans retinoic acid (ATRA; #R2625; Sigma) was added to LTR medium from day 20.

Generation of Tet-inducible NAIB integrated pluripotent stem cells. The NAIB construct was transfected into stem cells with dual reporters SIX6-H2b-eGFP and Brn3b-tdTomato. Additionally, the pY026 plasmid, which expresses huAsCpf1 and crRNA, was co-transfected into

the cells. Cells were electroporated at 1,300V for 20 ms. After transfection, cells were maintained in mTeSR with zeocin (200 ug/ml) for three weeks to select for the cells that had stably integrated the genetic cargo.

Direct conversion by activation of Tet-inducible expression of NAIB. Cells were passaged to single cell density using Accutase for 12 minutes at 37°C. Following this, cells were quenched with mTeSR and 5μM blebbistatin, pelleted at 80 x g for 5 minutes, resuspended in neural induction medium (NIM) with 5μM blebbistatin and 1μM of doxycycline. NIM consists of DMEM/F12, HEPES (#11330032; Life technologies), N2 supplement (#17502048; Life technologies), Non-essential amino acids (#11140050; Life technologies), and Gluta-MAX (#25030081; Life technologies). These cells were then plated at about 100,000 cells per well on a 12 well plate. After two days, cells were re-passaged in the same manner as stated above but this time, they were plated in differentiation medium with 5μM blebbistatin and 1μM of doxycycline and placed onto 24 well poly-L-ornithine (1mg/ml) coated plates at a density of 50,000 cells per well. Differentiation medium is comprised of Brain Phys (#05790; Stem Cell Technologies) and B27 supplement (#17504044; Life technologies). Cells were imaged in bright-field at 5x, 10x, and 20x fields of view to visualize neurite outgrowth. Fluorescence imaging using an ImageXpress microscope was carried out after three days to measure fluorescence intensity of Brn3b-Tomato. DAPI, Alexa Fluor 488, and Texas Red filters were used to visualize the BFP, GFP, and Tomato channels respectively.

Long-term survival in growth factor supplemented retinal ganglion cells. Additional growth factors and small molecules were added to the differentiation medium to attempt to optimize the efficiency of RGC differentiation and survival. In addition to 5μM blebbistatin, the media was supplemented with 10μM forskolin (MP Biomedicals; #109669-5MG) and 10ng/ml CNTF (R&D

systems; #257-NT) on day 2 after the first doxycycline treatment. Two days later, 50ng/ul BDNF (Peprotech #450-02-10µg) was added to the existing group of supplements.

FIGURES

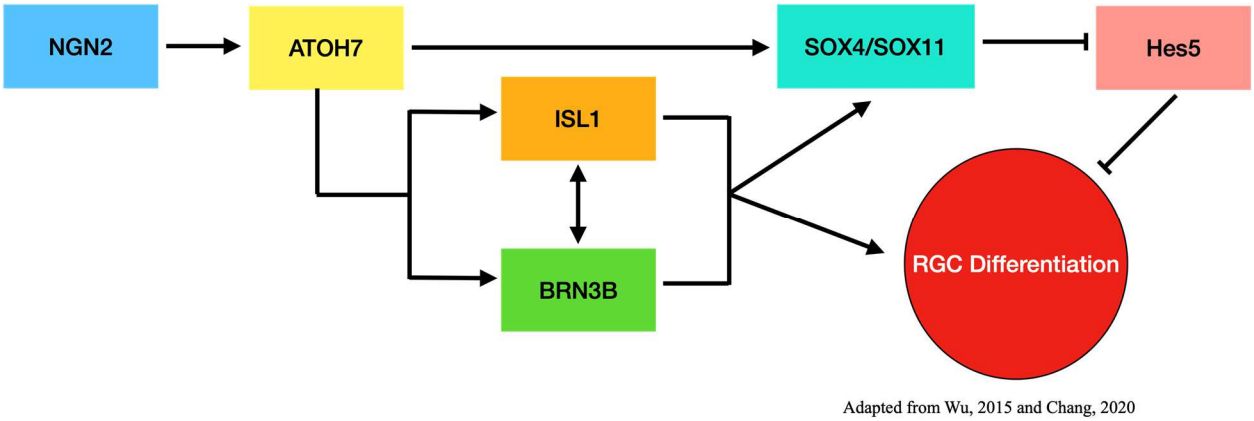

Figure 1: The interactions between the primary transcription factors involved in retinal ganglion cell differentiation. NGN2 was primarily for early neural induction but also activates the ATOH7 promoter which is a determining factor in RGC commitment. ATOH7 activates both ISL1 and BRN3B which drive the retinal progenitor cell to an RGC fate. It has also been shown that ATOH7 activates SOX4 and SOX11. SOX4/SOX11 have been shown to drive RGC differentiation and organization by inhibiting Hes5, a transcription factor known to inhibit RGC differentiation.

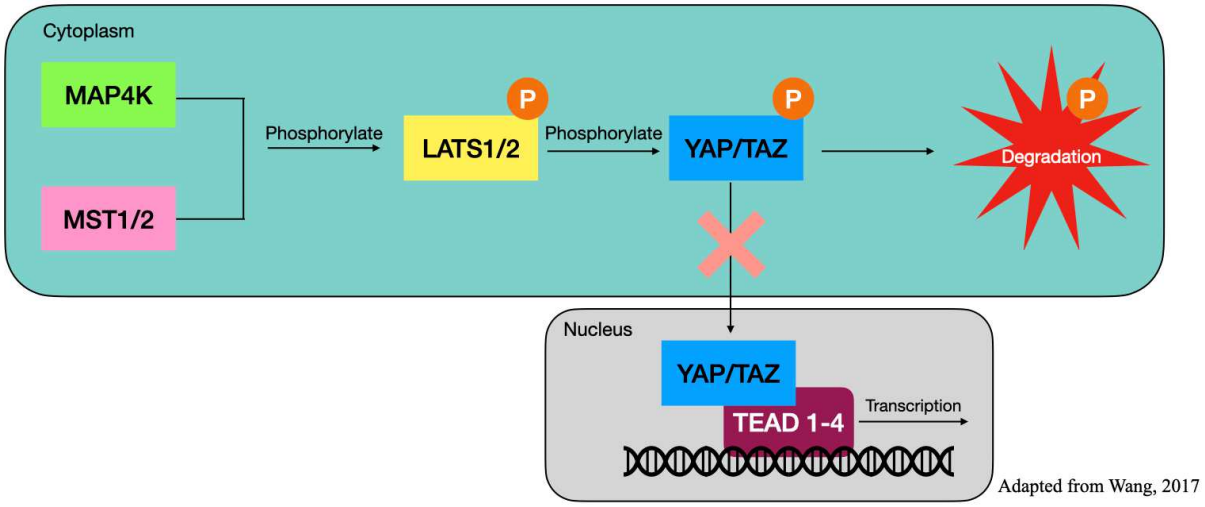

Figure 2: The mammalian Hippo signaling pathway and its components. MST1/2 and MAP4K both phosphorylate LATS1/2 which leads to the phosphorylation of YAP and TAZ. When YAP/TAZ are phosphorylated, they become inactivated and are subsequently degraded. When the Hippo pathway is downregulated, YAP/TAZ remains in an unphosphorylated state and translocates to the nucleus. There, they interact with TEAD 1-4 and regulate transcription.

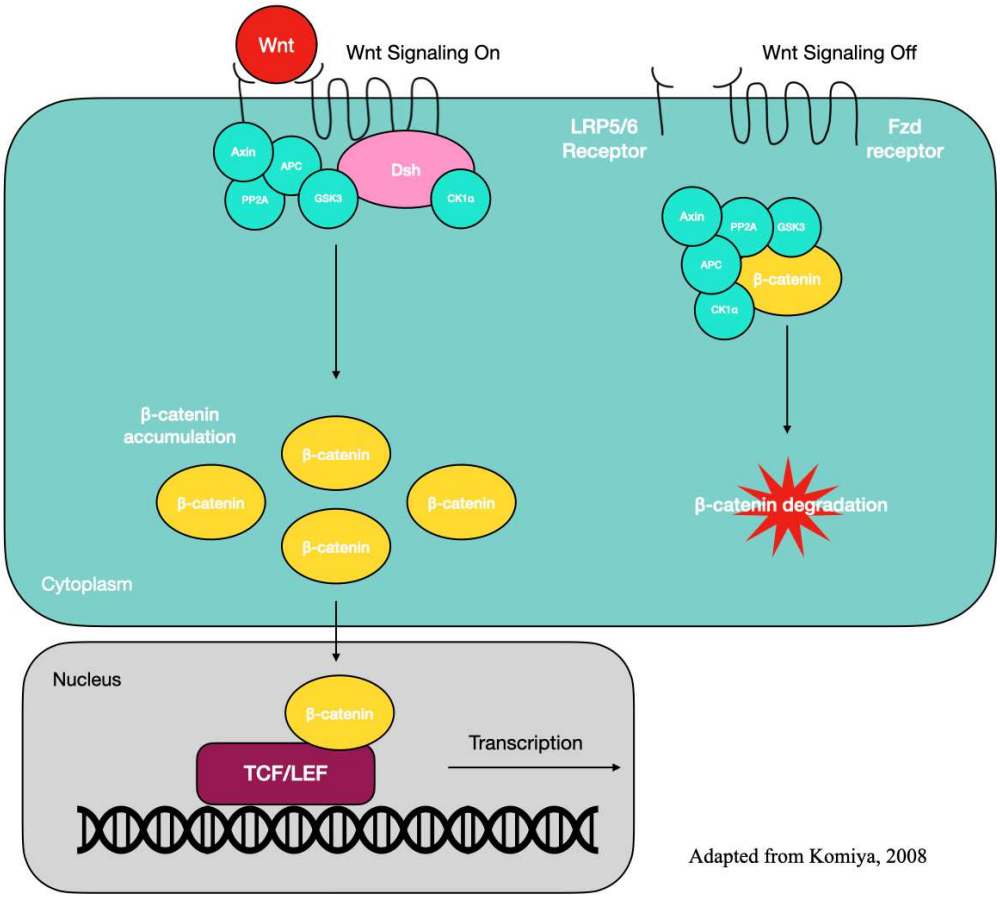

Figure 3: The canonical Wnt signaling pathway and its components. In the absence of Wnt, a complex composed of Axin, PP2A, APC, CK1α, and GSK3, binds to β-catenin and causes its degradation in the cytoplasm. When Wnt is present, it binds to the FZD and LRP5/6 receptors. Once Wnt is bound to these receptors, Axin binds to the LRP5/6 receptor and inactivates the β-catenin destruction complex. The phosphoprotein Dsh is activated by both CK1α and Axin and serves to downregulate GSK3 activity, causing a cascade whereby β-catenin is able to accumulate in the cytoplasm. Once β-catenin migrates to the nucleus, it complexes with TCF/LEF to regulate transcription.

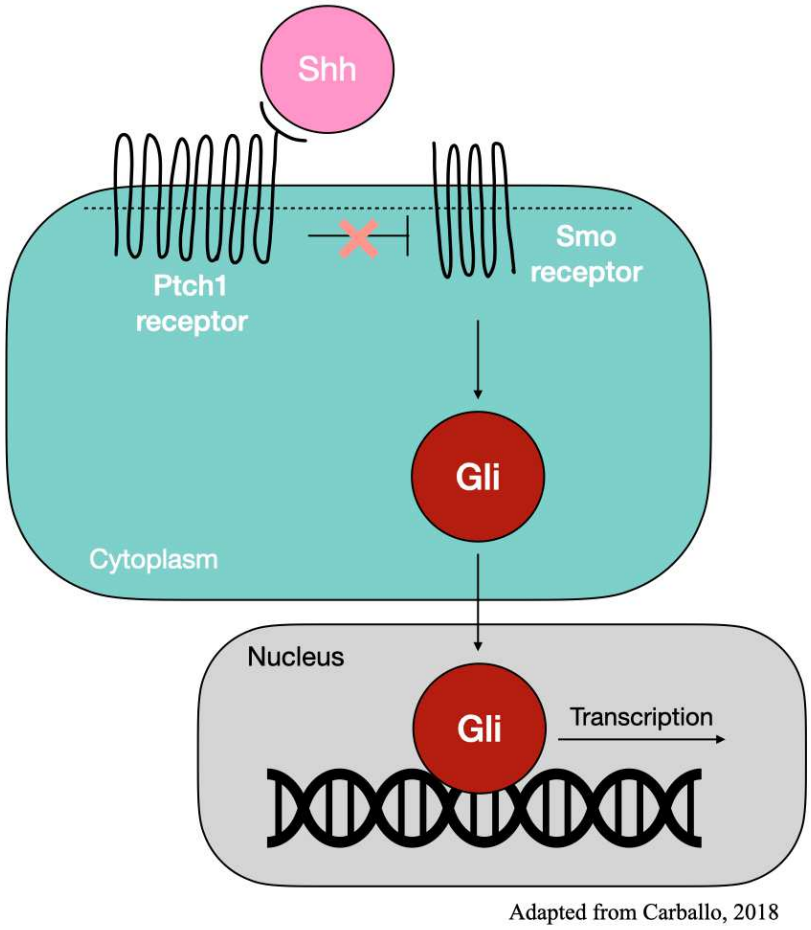

Figure 4: The canonical Sonic hedgehog signaling pathway and its components. The pathway begins with Shh binding to and inactivating Ptch1. Typically, Ptch1 represses the activity of Smo, so with Ptch1 inactivated, the activity of Smo is upregulated. This leads to several signaling cascades resulting a buildup of the protein Gli. Gli is then translocated to the nucleus where it regulates transcription.

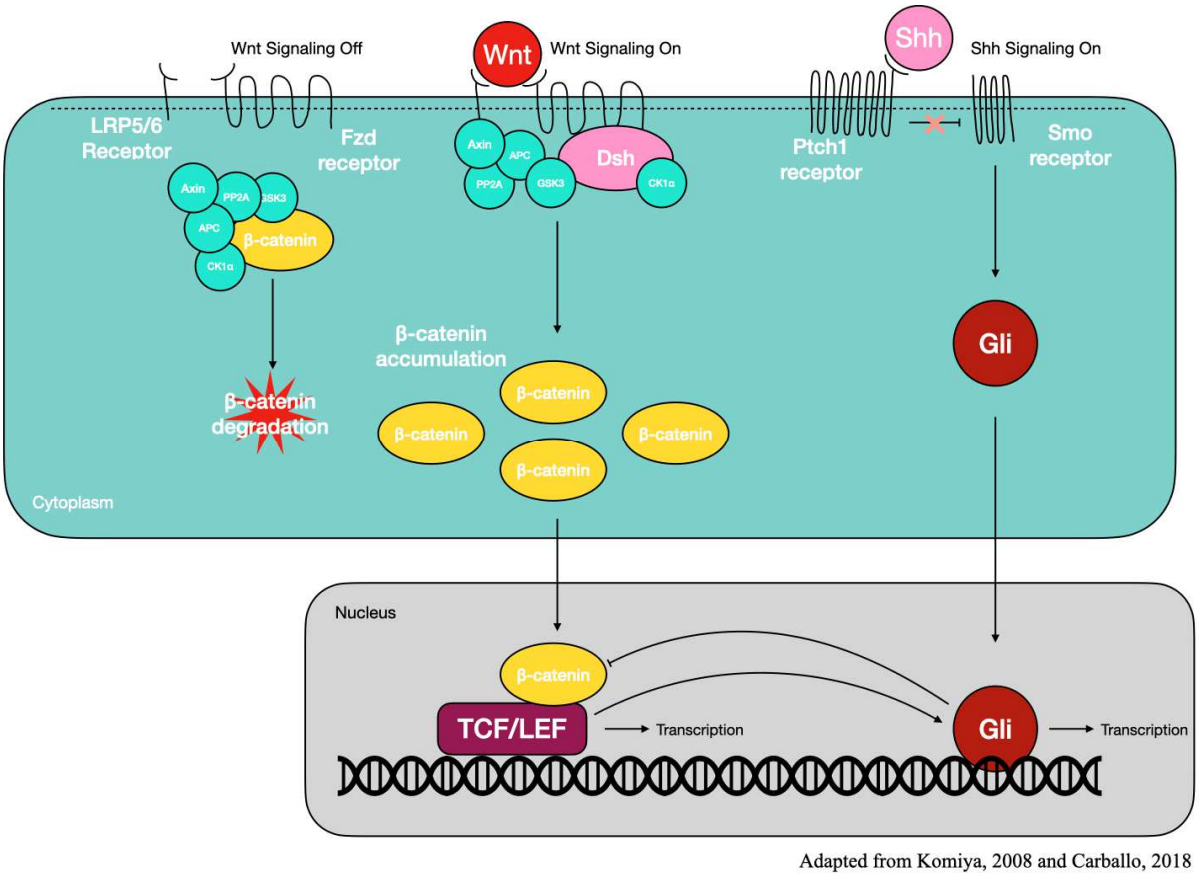

Adapted from Komiya, 2008 and Carballo, 2018

Figure 5: The canonical Wnt and Sonic hedgehog signaling pathways and their dynamic crosstalk interactions. In addition to regulating transcription in the nucleus, Gli inhibits the transcriptional ability of β-catenin. Further, TCF/LEF upregulates Gli in the nucleus.

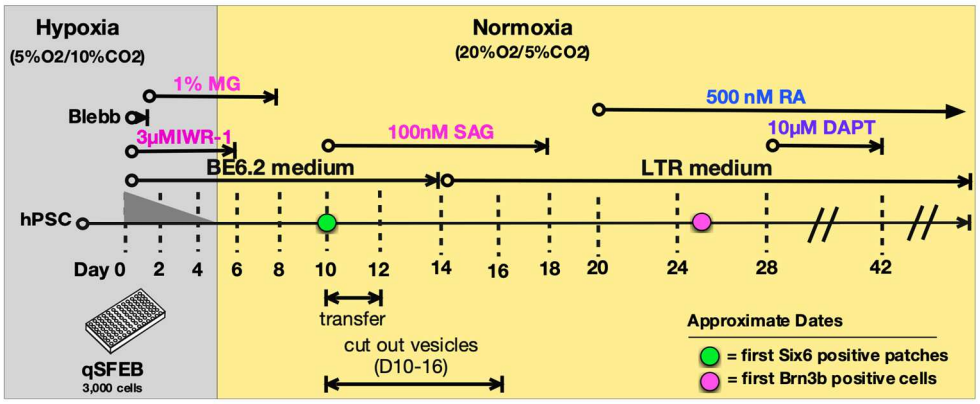

Figure 6: Schematic illustrating timeline for organoid differentiation. Broad overview of major checkpoints during organoid development. Cells are kept in hypoxia until day 5, after which they are transferred to normoxia. At day 14, cells are switched from BE6.2 media to LTR media. Various small molecules like Wnt inhibitor and Smoothened agonist are added to the media for specific periods to time to promote a retinal fate. Optic vesicles are cut from the growing organoid between day 10 and day 16 and they are transferred to another plate. Optic vesicle reporter *SIX6*-eGFP can first be seen on day 10 and ganglion cell marker Brn3b-tdTomato can first been seen on around day 25.

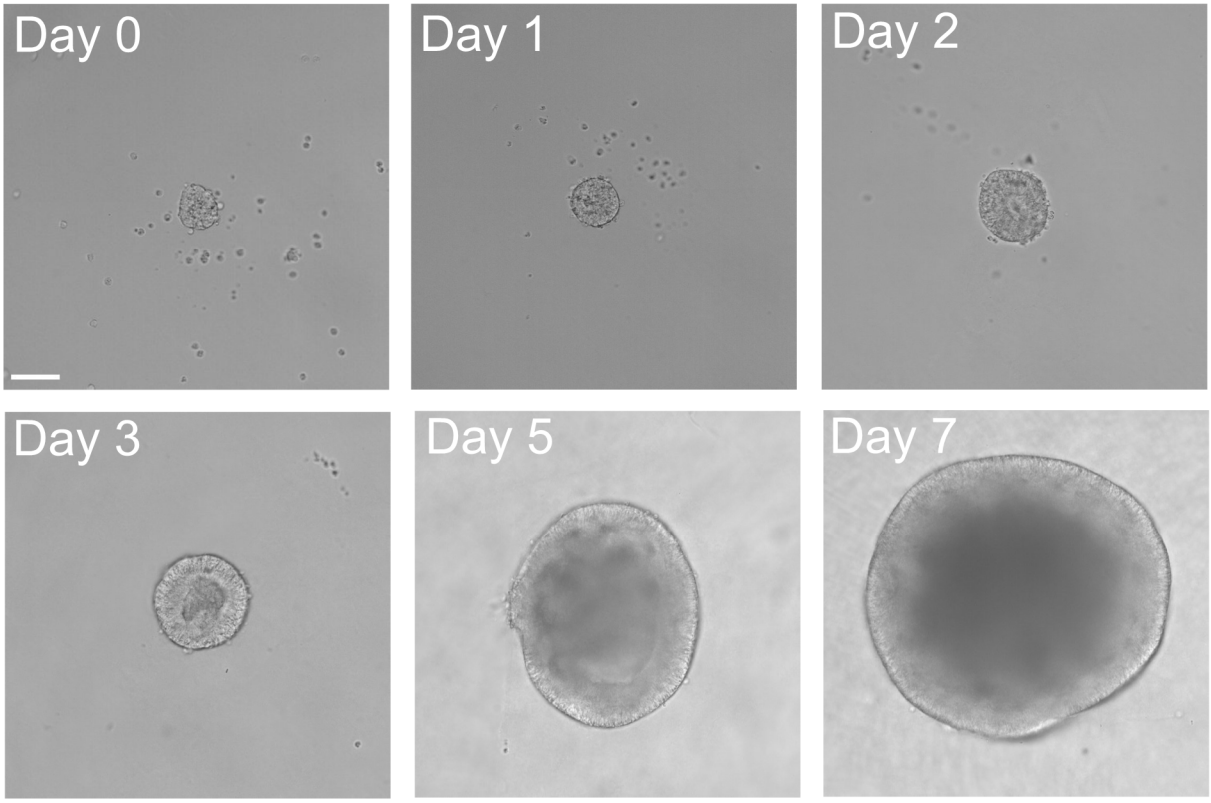

Figure 7: Forced aggregate differentiation of a single stem cell derived organoid monitored by live cell imaging. Pluripotent stem cell cultures were passaged to single cell density and 125 cells were placed into each well of a 96-well U-bottom plate and maintained in hypoxic conditions for 5 days. After 24 hours following dissociation, most cells aggregated into uniform spheres. The same organoid was tracked over time at a 10x field of view using a Molecular Devices ImageXpress. Scale bars = 125μm.

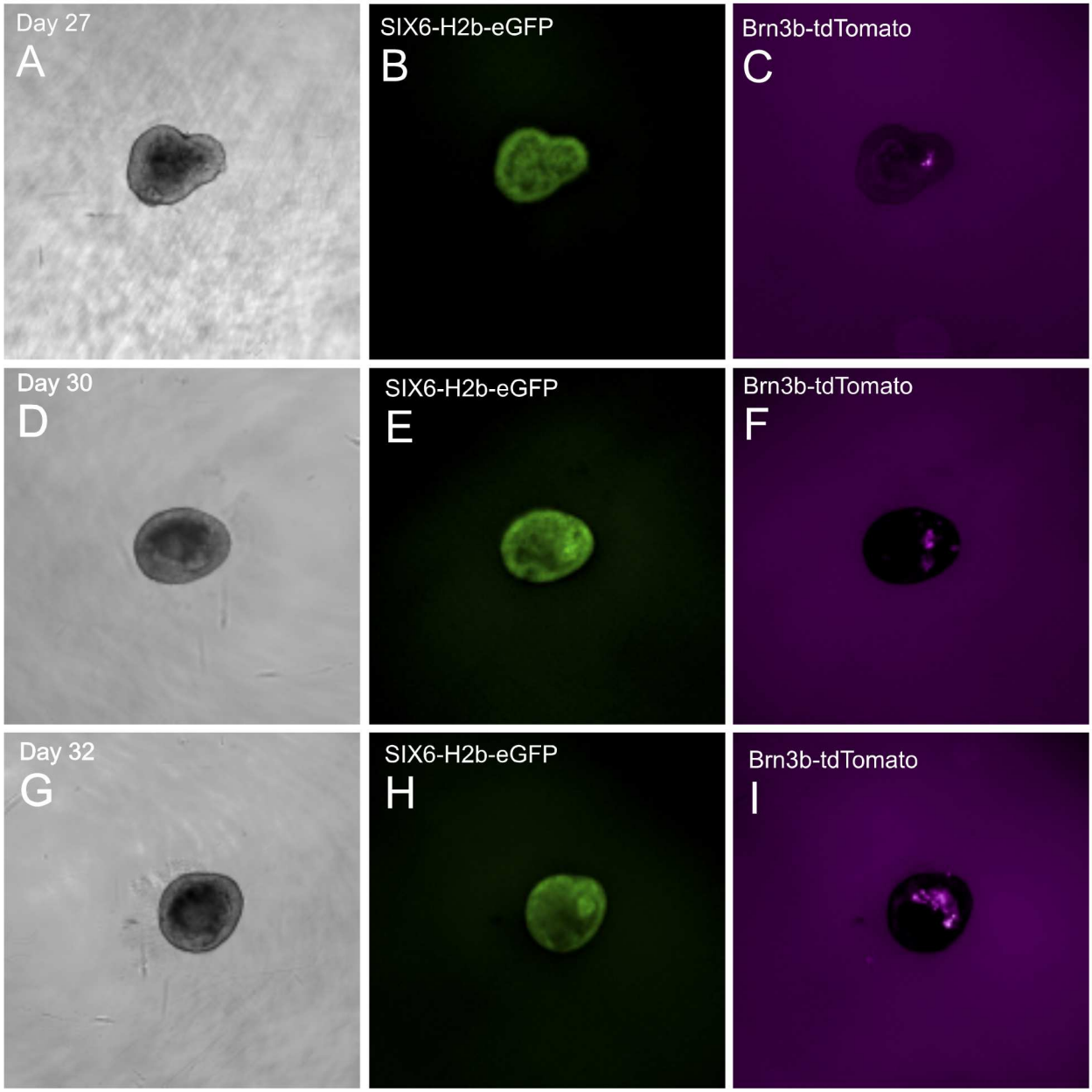

Figure 8: Demonstration of the SIX6-H2b-eGFP and Brn3b-tdTomato dual reporter in 3D retinal organoids. (A-C) Day 27 organoids express SIX6 but barely express BRN3B. (D-F) Day 30 organoids still express SIX6 and BRN3B expression is increasing but still low. (G-I) Day 32 organoids show consistent SIX6 expression but BRN3B expression continues to increase.

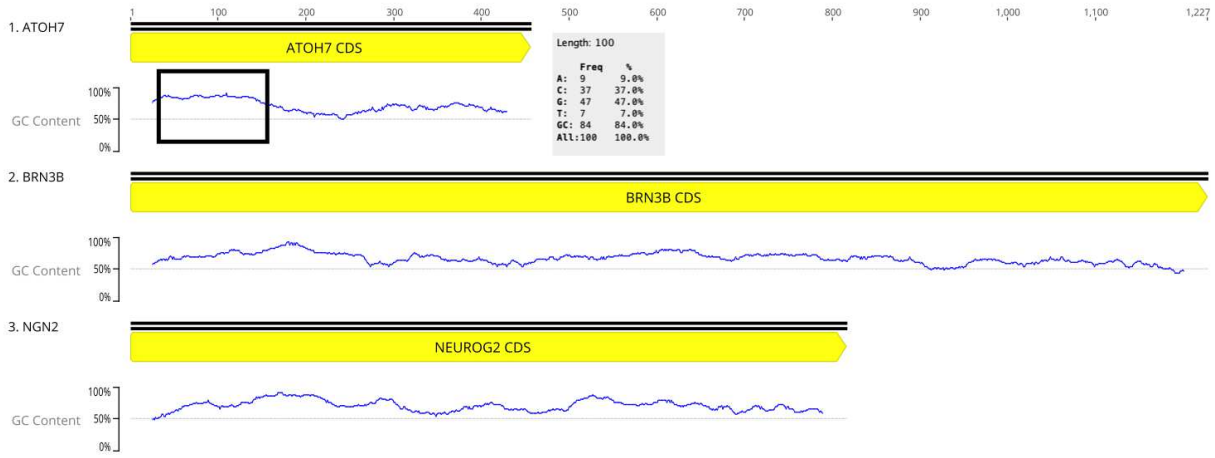

Figure 9: Graphical display of the GC content of genes amplified during NAIB construct assembly. Most of the genes in the NAIB cassette had a high GC content which created a challenge for assembly. In total, NGN2, ATOH7 and BRN3B has GC contents of approximately 69%, 70%, and 65% respectively. In some cases (e.g. ATOH7), the GC content exceeded 83% over at least 100 base pairs as seen above.

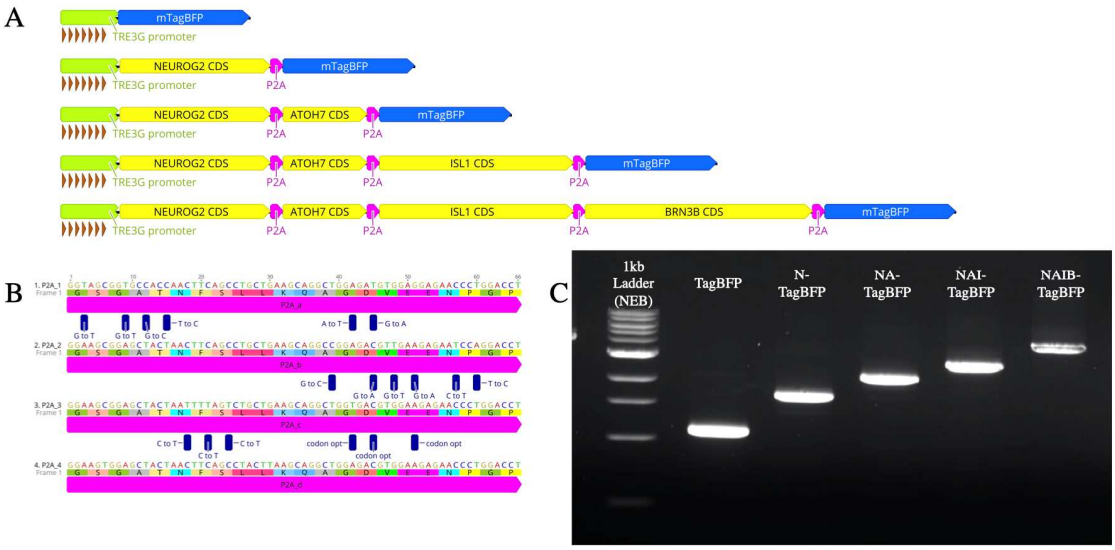

Figure 10: Visual representation of NAIB cassette assembly and verification via agarose gel electrophoresis. (A) The NAIB cassette was assembled via Gibson assembly in a sequential manner with P2A repeats separating them. (B) The P2A repeats spaced between each gene enables multiple genes to be synthesized from a single mRNA transcript. Each P2A sequence had specific base pair mutations which would enable some primer binding specificity at the nucleic acid level while leaving the amino acid sequence unchanged. (C) After the addition of each gene was added to the cassette, agarose gel electrophoresis was performed on the PCR product. The same primers were used for each PCR reaction, flanking the TRE3G promoter and the TagBFP. Here it is clear that with the addition of each new gene, the cassette grows in size.

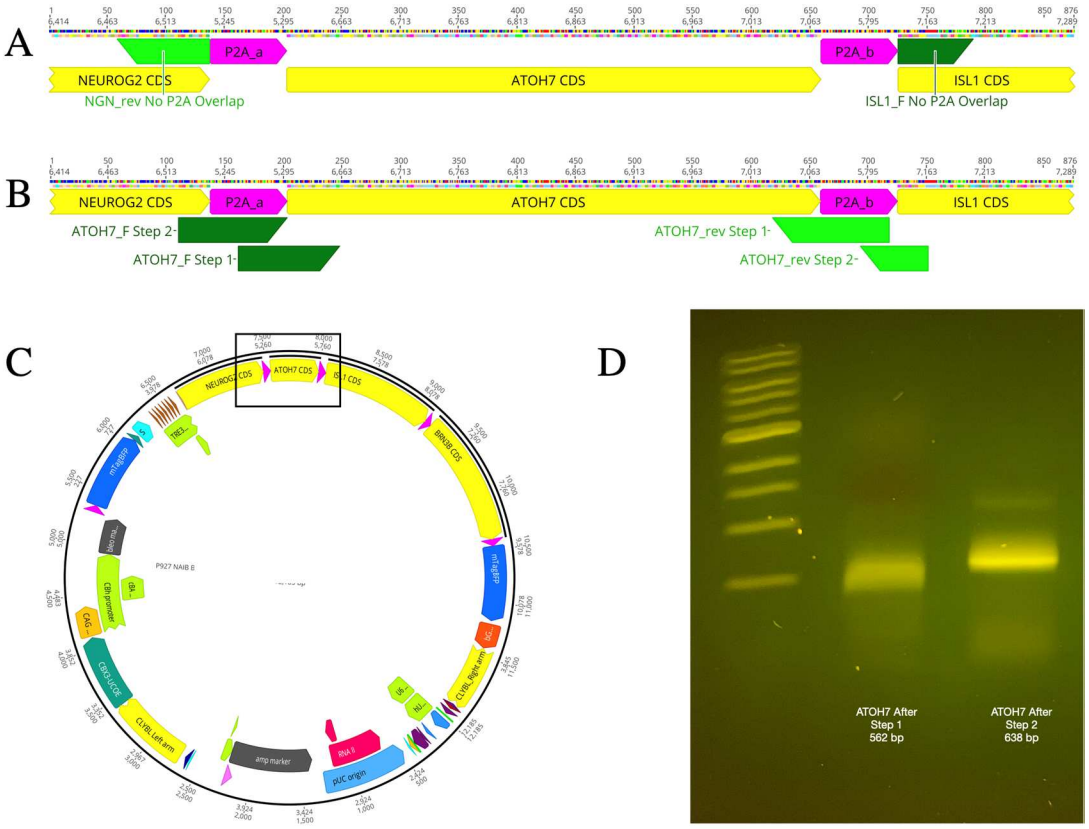

Figure 11: Example of 2-step PCR approach to amplify genes flanked by P2A repeats. (A) The primer set for the DNA backbone. Here, it was important that the primers had no overlap with the P2A repeats. Any overlap with the P2A sequences would lead to mispriming and make the shell amplification kinetically difficult. (B) The primer set for the ATOH7 gene insert amplification where the 2-step approach was used. The first step amplified ATOH7 from genomic DNA. The second step elongated the PCR product such that it had overlap with the PCR shell. (C) An overview of how the insert would fit into the DNA backbone serving as the shell. (D) Agarose gel electrophoresis evidence that the PCR product was elongated following the 2-step PCR approach.

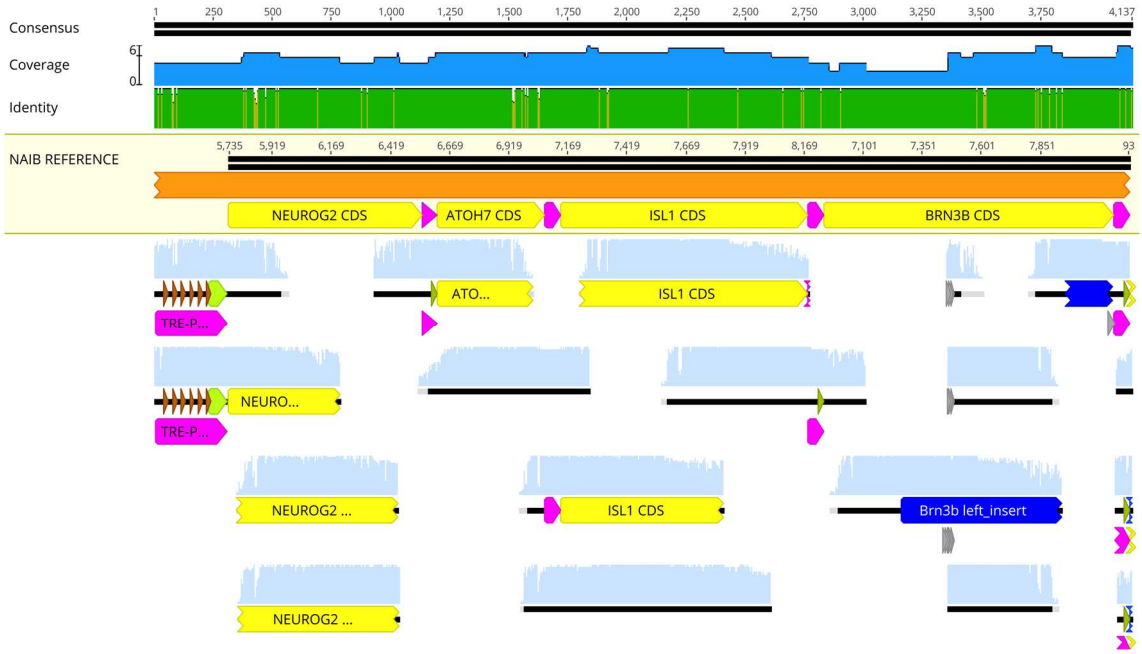

Figure 12: Sanger sequencing verification of the NAIB cassette. A contig assembly was generated using the Geneious software package (Biomatters) and aligned sequences were graphically represented to show overlap coverage between Sanger sequenced files and the expected NAIB reference sequence. Overlapping sequencing reactions were performed in a redundant fashion in order to ensure high quality reads and full coverage of newly synthesized gene fragments.

Figure 13: Design of the zeocin cassette preceding the NAIB cassette. This cassette is located directly before the tet inducible NAIB cassette and contains a constitutive Cbh promoter, a zeocin antibiotic resistance marker, a P2A repeat, and a TagBFP that localizes at the nucleus. The goal of this cassette is to enable the cells that successfully integrate the genetic cargo to be able to undergo antibiotic selection to quickly produce a pure population of transfected cells. The TagBFP is placed at the end of the cassette to give a visual fluorescent signal that the constitutive promoter is active, and the cell has a resistance to zeocin.

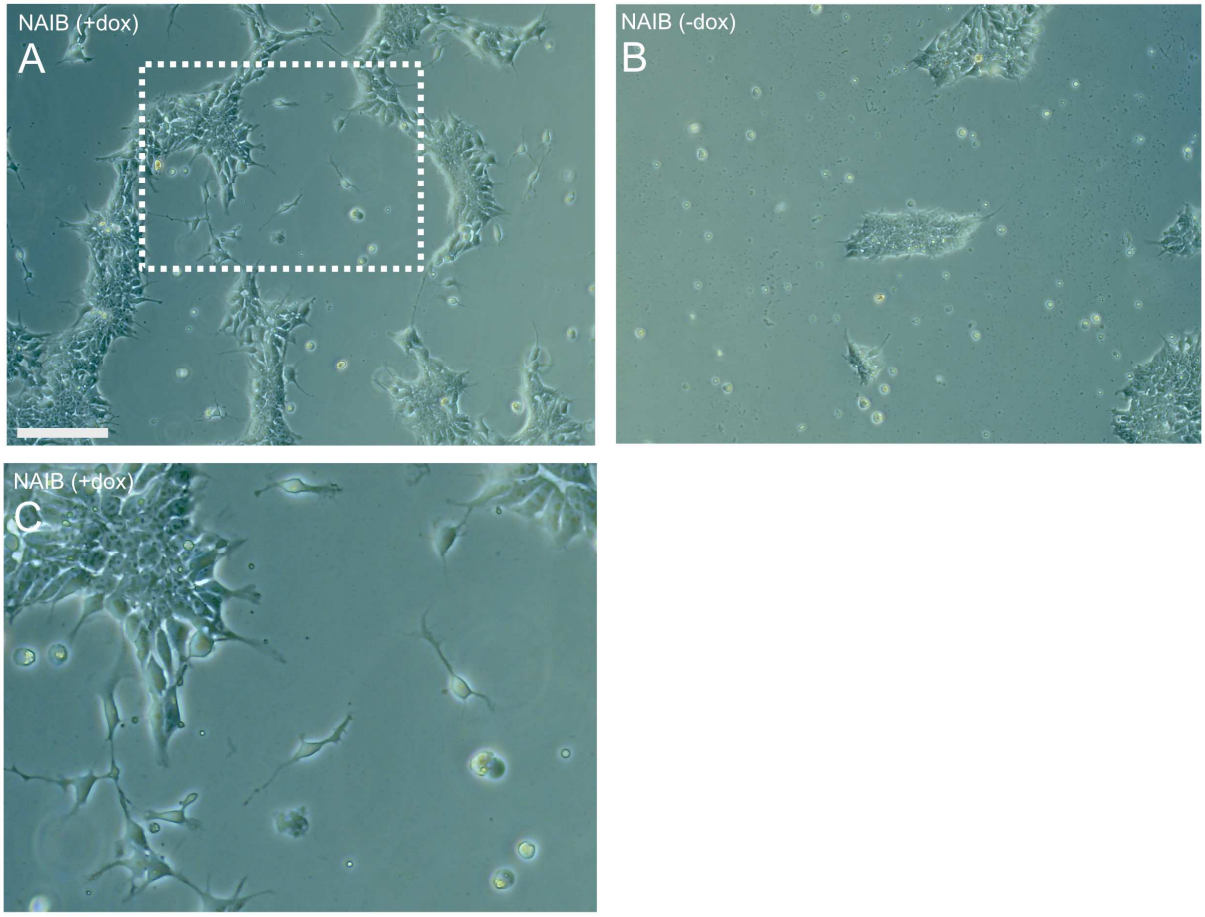

Figure 14: Transient transfection of the NAIB construct into human stem cells after doxycycline treatment for two days. (A and C) Cells that had been transiently transfected with NAIB and treated with doxycycline for two days demonstrated a shift towards a neuronal morphology. (B) The cells that were transiently transfected but not treated with doxycycline did not experience a morphological change and no neurons were observed. These neurons in the doxycycline treated samples were overrun by stem cells after a few days because not all of the cells had integrated the NAIB cassette and zeocin selection was not used. Scale bars = 100µm.

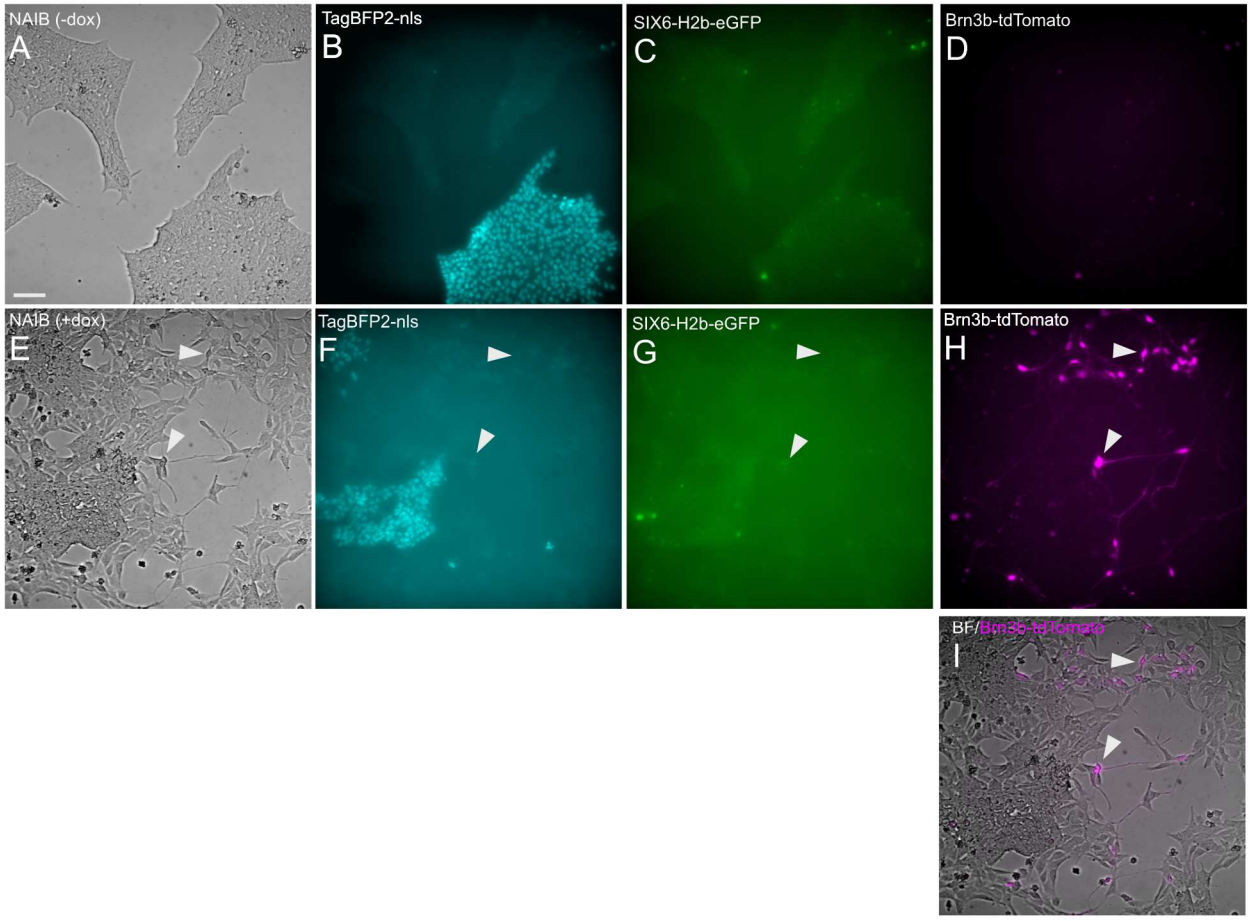

Figure 15: Comparing the morphology and gene expression of NAIB integrated cells with and without doxycycline. (A-D) Control stem cells with stable integration of a tet-inducible NAIB cassette and partially enriched by zeocin selection but not treated with dox. Here, the stem cell population is not entirely pure, but the NAIB integrated cells can be visualized with TagBFP2-nls (B). SIX6-H2b-eGFP was used to mark early retinal progenitors and Brn3b-tdTomato was used as an RGC marker. In this case, neither of these markers were active in the cells not treated with doxycycline. (E-H) Cells transfected with the NAIB cassette and zeocin selected. Cells were then treated with doxycycline for three days. Like in the non-doxycycline sample, many of the cells showed a positive TagBFP2-nls signal indicating integration of the genetic cargo into the cells (F). However, unlike the other sample, the sample treated with doxycycline did show some SIX6 expression and BRN3B expression (G-H). Importantly, the neurons that displayed a change in morphology expressed all three fluorescent channels. Arrows indicate cells that demonstrate fluorescence colocalization. (I) Merged bright-field and Brn3b-tdTomato channels illustrating the neuronal morphology aligning with the ganglion cell marker. Scale bars = 75µm.

Table 1: Cloning oligonucleotides for NAIB construct creation.

Gene Name	NAME	Sequence
NGN2	C1572 tet_NEUROG2_multi_F	AGAGCTCGTTTAGTGAACCGTCAGATCGCCAC CATGTTCGTCAAATCCGAGACCTTGGAGTTGA AGGAGGAAGAGGACG
	C1966_NGN2_CDS_rev2	GATACAATCCCTGGCTATGGGGAGGTGAGGTG CATAGCGGTGCTTGTCGGGAGGTGGGGGCTGC CAATAGTCCATGTCT
ATOH7	C1704_v3-NGN2-ATOH7p2aFIX_F	CTGCTGAAGCAGGCTGGAGATGTGGAGGAGA ACCCTGGACCTATGAAGTCCTGCAAGCCCAGC GGCCCGCCGGCGGGAGCGCGCGTT
	C1973_ ATOH7_Overlap2_F	CACCTCCCCATAGCCAGGGATTGTATCGGTAG CGGTGCCACCAACTTCAGCCTGCTGAAGCAGG CTGGAGATGTGGAGGAGAACCCTGGACCT
	C1705_v3-ATOH7-p2aTagBFPfixRev2	GGATTCTCTTCAACGTCTCCGGCCTGCTTCAGC AGGCTGAAGTTAGTAGCTCCGCTTCCGGTGGC CATCTGGAAGGGCTCGGGCTGGAAGCCGAAG AGTC
	C1972_ATOH7_Overlap2_Rev	TTTGGTGGATCTCCCATGTCTCCCATAGGTCCT GGATTCTCTTCAACGTCTCCGGCCT
ISL1	C1941_ATOH7_shell_Fv2	ATGGGAGACATGGGAGATCCACCAAAAAAAA AACGTCTGATTTCCCTATGTGTTGGTTGCGGCA
	C1961_ISL_CDS_rev	TGCCTCAATAGGACTGGCTACCATGCTGTTAG GTGTATCTGGAAGT
BRN3B	C1955_Brn3b_CDS_F	ATGATGATGATGTCCCTGAACAGCAAGCAGGC GTTTAGCATGCCGC
	C1563_BRN3B_donor_shell_rev	ATGCCGGCGGAATATTTCATTCTTTTCTGTTTC TGCCTCT
TagBFP2	C1946_TagBFP_noATG_F	GTGTCTAAGGGCGAAGAGCTGATTAAGGAGA ACATGCACATGAAGCTGT
	C1270_NLS_bGH_rev	GCTCTAGTTAGAATTCCTTTTTCTTTTTTGCCTG GCCGGCCTTTTTCGTGGCCGCCGGCCTTTTATT AAGCTTGTGCCCCAGTTTG
ieSpCas9	C676_Cas9backbone_F	GACCTGTCTCAGCTGGGAGGCGACAAAAGGCC GGCGGCCACGAAA
	C679_Cas9backbone_R	GGCCGATGCTGTACTTCTTGTCGGCTGCTGGG ACTCCGTGGATAC
	C675_Cas9insert_for	GACAAGAAGTACAGCATCGGCCTGGACATCGG CACCAACT
	C677_Cas9insert_rev	GTCGCCTCCCAGCTGAGACAGGTCGATCCGTG TCTCGTAC
eSpCas9	C851_hU6prom_fwd	AGGCGCCTAGGGAATTCGCGGCCGCCTTTTGC TCACATGTGAGGGC
	C233_hU6prom_rev	TTACCCCAGTTGGGGTCGCGGCCGCCAAAAAA GCACCGACTCGGT

REFERENCES

1. Adler R, Canto-Soler MV. Molecular mechanisms of optic vesicle development: Complexities, ambiguities and controversies. *Developmental Biology*. 2007;305(1):1-13. doi:10.1016/j.ydbio.2007.01.045

2. Albert S, Müller F, Fischer N, Biellmann D, Neumann C, Blader P, Strähle U. Cyclops-independent floor plate differentiation in zebrafish embryos. *Developmental Dynamics*. 2003;226(1):59-66. doi:10.1002/dvdy.10211

3. Baden T, Euler T, Berens P. Understanding the retinal basis of vision across species. *Nat Rev Neurosci*. 2020;21(1):5-20. doi:10.1038/s41583-019-0242-1

4. Beffagna G. Zebrafish as a Smart Model to Understand Regeneration After Heart Injury: How Fish Could Help Humans. *Front Cardiovasc Med*. 2019;6. doi:10.3389/fcvm.2019.00107

5. Busskamp V, Lewis NE, Guye P, Ng AH, Shipman SL, Byrne SM, Sanjana NE, Murn J, Li Y, Li S, Stadler M, Weiss R, Church GM. Rapid neurogenesis through transcriptional activation in human stem cells. *Mol Syst Biol*. 2014;10(11):760. doi:10.15252/msb.20145508

6. Carballo GB, Honorato JR, de Lopes GPF, Spohr TCL de S e. A highlight on Sonic hedgehog pathway. *Cell Commun Signal*. 2018;16(1):11. doi:10.1186/s12964-018-0220-7

7. Chang K-C, Hertz J. SoxC transcription factors in retinal development and regeneration. *Neural Regen Res*. 2017;12(7):1048. doi:10.4103/1673-5374.211178

8. Conte I, Morcillo J, Bovolenta P. Comparative analysis of *Six3* and *Six6* distribution in the developing and adult mouse brain. *Dev Dyn*. 2005;234(3):718-725. doi:10.1002/dvdy.20463

9. Costamagna D, Mommaerts H, Sampaolesi M, Tylzanowski P. Noggin inactivation affects the number and differentiation potential of muscle progenitor cells in vivo. *Scientific Reports*. 2016;6(1):31949. doi:10.1038/srep31949

10. Daniels RW, Rossano AJ, Macleod GT, Ganetzky B. Expression of Multiple Transgenes from a Single Construct Using Viral 2A Peptides in Drosophila. McCabe BD, ed. *PLoS ONE*. 2014;9(6):e100637. doi:10.1371/journal.pone.0100637

11. De Los Angeles A, Ferrari F, Xi R, Fujiwara Y, Benvenisty N, Deng H, Hochedlinger K, Jaenisch R, Lee S, Leitch HG, Lensch MW, Lujan E, Pei D, Rossant J, Wernig M, Park PJ, Daley GQ. Hallmarks of pluripotency. *Nature*. 2015;525(7570):469-478. doi:10.1038/nature15515

12. Fuhrmann S. Eye Morphogenesis and Patterning of the Optic Vesicle. In: *Current Topics in Developmental Biology*. Vol 93. Elsevier; 2010:61-84. doi:10.1016/B978-0-12-385044-7.00003-5

13. Giger FA, Houart C. The Birth of the Eye Vesicle: When Fate Decision Equals Morphogenesis. *Front Neurosci*. 2018;12:87. doi:10.3389/fnins.2018.00087

14. Gorsuch RA, Lahne M, Yarka CE, Petravick ME, Li J, Hyde DR. Sox2 regulates Müller glia reprogramming and proliferation in the regenerating zebrafish retina via Lin28 and Ascl1a. *Exp Eye Res*. 2017;161:174-192. doi:10.1016/j.exer.2017.05.012

15. Grath A, Dai G. Direct cell reprogramming for tissue engineering and regenerative medicine. *J Biol Eng*. 2019;13(1):14. doi:10.1186/s13036-019-0144-9

16. Heavner W, Pevny L. Eye Development and Retinogenesis. *Cold Spring Harbor Perspectives in Biology*. 2012;4(12):a008391-a008391. doi:10.1101/cshperspect.a008391

17. Henry JJ, Tsonis PA. Molecular and cellular aspects of amphibian lens regeneration. *Progress in Retinal and Eye Research*. 2010;29(6):543-555. doi:10.1016/j.preteyeres.2010.07.002

18. Hufnagel RB, Le TT, Riesenberg AL, Brown NL. Neurog2 controls the leading edge of neurogenesis in the mammalian retina. *Developmental Biology*. 2010;340(2):490-503. doi:10.1016/j.ydbio.2010.02.002

19. Isenmann S. Molecular determinants of retinal ganglion cell development, survival, and regeneration. *Progress in Retinal and Eye Research*. 2003;22(4):483-543. doi:10.1016/S1350-9462(03)00027-2

20. Jiang Y, Ding Q, Xie X, Libby RT, Lefebvre V, Gan L. Transcription Factors SOX4 and SOX11 Function Redundantly to Regulate the Development of Mouse Retinal Ganglion Cells. *J Biol Chem*. 2013;288(25):18429-18438. doi:10.1074/jbc.M113.478503

21. Komiya Y, Habas R. Wnt signal transduction pathways. *Organogenesis*. 2008;4(2):68-75. doi:10.4161/org.4.2.5851

22. Levin LA, Gordon LK. Retinal ganglion cell disorders: types and treatments. *Progress in Retinal and Eye Research*. 2002;21(5):465-484. doi:10.1016/S1350-9462(02)00012-5

23. Luo Z, Xu C, Li K, Xian B, Liu Y, Li K, Liu Y, Rong H, Tang M, Hu D, Yang S, Ye M, Zhong X, Ge J. Islet1 and Brn3 Expression Pattern Study in Human Retina and hiPSC-Derived Retinal Organoid. *Stem Cells International*. 2019;2019:1-14. doi:10.1155/2019/8786396

24. Maddaluno L, Urwyler C, Werner S. Fibroblast growth factors: key players in regeneration and tissue repair. *Development*. 2017;144(22):4047-4060. doi:10.1242/dev.152587

25. Madelaine R, Mourrain P. Endogenous retinal neural stem cell reprogramming for neuronal regeneration. *Neural Regen Res*. 2017;12(11):1765. doi:10.4103/1673-5374.219028

26. Marques IJ, Lupi E, Mercader N. Model systems for regeneration: zebrafish. *Development*. 2019;146(18):dev167692. doi:10.1242/dev.167692

27. Masri R. Neurons of the primate retina: A qualitative and quantitative analysis. Published online April 4, 2019. Accessed August 16, 2020. https://ses.library.usyd.edu.au/handle/2123/21165

28. Quigley HA. Neuronal death in glaucoma. *Progress in Retinal and Eye Research*. 1999;18(1):39-57. doi:10.1016/S1350-9462(98)00014-7

29. Rueda EM, Hall BM, Hill MC, Swinton PG, Tong X, Martin JF, Poché RA. The Hippo Pathway Blocks Mammalian Retinal Müller Glial Cell Reprogramming. *Cell Reports*. 2019;27(6):1637-1649.e6. doi:10.1016/j.celrep.2019.04.047

30. Schiller PH, Sandell JH, Maunsell JHR. Functions of the ON and OFF channels of the visual system. *Nature*. 1986;322(6082):824-825. doi:10.1038/322824a0

31. Schnapp E. Hedgehog signaling controls dorsoventral patterning, blastema cell proliferation and cartilage induction during axolotl tail regeneration. *Development*. 2005;132(14):3243-3253. doi:10.1242/dev.01906

32. Takahashi K, Yamanaka S. Induction of Pluripotent Stem Cells from Mouse Embryonic and Adult Fibroblast Cultures by Defined Factors. *Cell*. 2006;126(4):663-676. doi:10.1016/j.cell.2006.07.024

33. Vergara MN, Del Rio-Tsonis K. Retinal regeneration in the Xenopus laevis tadpole: a new model system. *Mol Vis*. 2009;15:1000-1013.

34. Wahlin KJ, Maruotti JA, Sripathi SR, Ball J, Angueyra JM, Kim C, Grebe R, Li W, Jones BW, Zack DJ. Photoreceptor Outer Segment-like Structures in Long-Term 3D Retinas from Human Pluripotent Stem Cells. *Scientific Reports*. 2017;7(1):766. doi:10.1038/s41598-017-00774-9

35. Wan J, Goldman D. Retina regeneration in zebrafish. *Current Opinion in Genetics & Development*. 2016;40:41-47. doi:10.1016/j.gde.2016.05.009

36. Wang C, Ward ME, Chen R, Liu K, Tracy TE, Chen X, Xie M, Sohn PD, Ludwig C, Meyer-Franke A, Karch CM, Ding S, Gan L. Scalable Production of iPSC-Derived Human Neurons to Identify Tau-Lowering Compounds by High-Content Screening. *Stem Cell Reports*. 2017;9(4):1221-1233. doi:10.1016/j.stemcr.2017.08.019

37. Wang RN, Green J, Wang Z, Deng Y, Qiao M, Peabody M, Zhang Q, Ye J, Yan Z, Denduluri S, Idowu O, Li M, Shen C, Hu A, Haydon RC, Kang R, Mok J, Lee MJ, Luu HL, Shi LL. Bone Morphogenetic Protein (BMP) signaling in development and human diseases. *Genes & Diseases*. 2014;1(1):87-105. doi:10.1016/j.gendis.2014.07.005

38. Wang Y, Yu A, Yu F-X. The Hippo pathway in tissue homeostasis and regeneration. *Protein Cell*. 2017;8(5):349-359. doi:10.1007/s13238-017-0371-0

39. Weinreb RN, Aung T, Medeiros FA. The Pathophysiology and Treatment of Glaucoma: A Review. *JAMA*. 2014;311(18):1901. doi:10.1001/jama.2014.3192

40. Whyte JL, Smith AA, Helms JA. Wnt Signaling and Injury Repair. *Cold Spring Harbor Perspectives in Biology*. 2012;4(8):a008078-a008078. doi:10.1101/cshperspect.a008078

41. Wu F, Kaczynski TJ, Sethuramanujam S, Li R, Jain V, Slaughter M, Mu X. Two transcription factors, Pou4f2 and Isl1, are sufficient to specify the retinal ganglion cell fate. *Proc Natl Acad Sci USA*. 2015;112(13):E1559-E1568. doi:10.1073/pnas.1421535112

42. Xia H, Li X, Gao W, Fu X, Fang RH, Zhang L, Zhang K. Tissue repair and regeneration with endogenous stem cells. *Nat Rev Mater*. 2018;3(7):174-193. doi:10.1038/s41578-018-0027-6

43. Xiang M, Jiang H, Jin K, Qiu F. Molecular Control of Retinal Ganglion Cell Specification and Differentiation. In: Rumelt S, ed. *Glaucoma - Basic and Clinical Concepts*. InTech; 2011. doi:10.5772/19832

44. Xiao D, Qiu S, Huang X, Zhang R, Lei Q, Huang W, Chen H, Gou B, Tie X, Liu S, Liu Y, Jin K, Xiang M. *Directed Robust Generation of Functional Retinal Ganglion Cells from Müller Glia*. Neuroscience; 2019. doi:10.1101/735357

45. Yamada ES, Bordt AS, Marshak DW. Wide-field ganglion cells in macaque retinas. *Vis Neurosci*. 2005;22(4):383-393. doi:10.1017/S095252380522401X

46. Yu L, Han M, Yan M, Lee E-C, Lee J, Muneoka K. BMP signaling induces digit regeneration in neonatal mice. *Development*. 2010;137(4):551-559. doi:10.1242/dev.042424

47. Zhang C-W, Lu Q, You S-W, Zhi Y, Yip HK, Wu W, So K-F, Cui Q. CNTF and BDNF have similar effects on retinal ganglion cell survival but differential effects on nitric oxide synthase expression soon after optic nerve injury. *Invest Ophthalmol Vis Sci*. 2005;46(4):1497-1503. doi:10.1167/iovs.04-0664

48. CRISPR 101 | The Simple Guide to Learning CRISPR. Accessed August 16, 2020. https://www.synthego.com/resources/crispr-101-ebook